Electron-Transfer Kinetics and Electrostatic Properties of the *Rhodobacter sphaeroides* Reaction Center and Soluble *c*-Cytochromes†

David M. Tiede,*,‡ Annie-Claude Vashishta,‡ and M. R. Gunner§

Chemistry Division, Argonne National Laboratory, Argonne, Illinois 60439, and Department of Physics, City College of New York, New York, New York 10031

Received December 18, 1992; Revised Manuscript Received February 9, 1993

ABSTRACT: The kinetics of electron transfer between the *Rhodobacter sphaeroides* R-26 reaction center and nine soluble *c*-cytochromes have been analyzed and compared to the patterns of the surface electrostatic potentials for each of the proteins. Characteristic first-order electron-transfer rates for 1:1 complexes formed at low ionic strength between the reaction center and the different *c*-cytochromes were identified and found to vary by a factor of almost 100, while second-order rates were found to differ by greater than 10^6. A correlation was found between the location of likely electrostatic interaction domains on each cytochrome and its characteristic rate of electron transfer. The interaction domains were identified by mapping electrostatic potentials, calculated from the Poisson–Boltzmann equation, onto simulated "encounter surfaces" for each of the cytochromes and the reaction center. For the reaction center, the *c*-cytochrome binding domain was found to have almost exclusively net negative potential (<–3 kT) and to be shifted slightly toward the M-subunit side of the reaction center. The location of interaction domains of complementary, positive potential (>3 kT) differed for each cytochrome. The correspondence between electrostatic, structural, and kinetic properties of 1:1 reaction center–cytochrome complexes leads to a proposed mechanism for formation of reaction center–cytochrome electron-transfer complexes that is primarily driven by the juxtaposition of regions of delocalized complementary potential. In this mechanism the clustering of charged residues is of primary importance and not the location of specific residues. A consequence of this mechanism is that many different sets of charge distributions are predicted to be capable of stabilizing a specific configuration for a reaction center–cytochrome complex. This mechanism for reaction center association with water-soluble *c*-cytochromes fits molecular recognition mechanisms proposed for *c*-cytochromes in nonphotosynthetic systems. In general, the kinetic scheme for reaction center driven cytochrome oxidation was found to vary between a simple two-state model, involving cytochrome in free and reaction center bound states, and a three-state model, that includes cytochrome binding in kinetically competent ("proximal") and incompetent ("distal") modes. The kinetically incompetent mode of cytochrome binding is suggested not to be an intrinsic feature of the reaction center–cytochrome association but is likely to be due to variation in the physical state of the reaction center.

The oxidation of water-soluble *c*-cytochromes by the *Rhodobacter sphaeroides* reaction center has provided a useful experimental system for investigations into the mechanisms of bimolecular electron transfer. The reaction center was the first reaction partner where *c*-cytochrome oxidation could be examined with single-turnover kinetics (Dutton et al., 1975; Moser & Dutton, 1988). The resolution of the *Rb. sphaeroides* R-26 reaction center crystal structure (Allen et al., 1986, 1987; Chang et al., 1991; El-Kabbani et al., 1991; Tiede et al., 1988), combined with the knowledge of several cytochrome structures (Bhatia, 1981; Bushnell et al., 1990; Holden et al., 1987; Louie & Brayer, 1990; Louie et al., 1988; Matsuura et al., 1982; Salemme et al., 1973; Takano & Dickerson, 1981), allows the mechanism for the formation of transient electron-transfer complexes between the reaction center and the *c*-cytochromes to be addressed with atomic detail.

Electron transfer occurs from ferrous cytochrome *c* to the light-generated, cation free radical of the bacteriochlorophyll dimer, P^+, in the reaction center. The P^+ state is formed with a reaction time of 3 ps following laser excitation and has a lifetime on the seconds time scale in the presence of excess quinone acceptors (Gunner, 1991). Subsequent single-turnover electron-transfer kinetics from the cytochrome to P^+ have been well-studied in vivo and in vitro. Cytochrome c_2 oxidation in *Rb. sphaeroides* cells and intact membrane is strongly biphasic, with nearly equal extents of two components having reaction times of 1–4 and 100–400 μs (Dutton et al., 1975; Joliot et al., 1989; Overfield et al., 1979). One interpretation attributes the multiphasic kinetics to two different modes of cytochrome binding to the reaction center, termed "proximal" and "distal", that yield fast and slow kinetic phases, respectively (Dutton et al., 1975; Dutton & Prince, 1978). A more recent analysis of P^+ reduction kinetics as a function of light saturation suggests that the multiphasic in vivo kinetics are not due to multiple modes of binding of the cytochrome to the reaction center but instead arise from the association of two reaction centers and one ubiquinone–cytochrome *c* oxidoreductase in a "supercomplex" in the intact membrane (Joliot et al., 1989; Lavergne & Joliot, 1991). The data suggest that the reaction centers are associated in a manner such that the binding of cytochrome on one reaction center competitively inhibits binding at the other (Joliot et al., 1989; Lavergne & Joliot, 1991).

In contrast to the general agreement on the kinetic format measured for cytochrome oxidation in vivo, different kinetic results have been reported for reaction center driven cyto-

† This work was supported, in part (D.M.T. and A.-C.V.), by the U.S. Department of Energy, Office of Basic Energy Sciences, Division of Chemical Sciences, under Contract W-31-109-Eng-38.

* Address correspondence to this author.
‡ Argonne National Laboratory.
§ City College of New York.

0006-2960/93/0432-4515$04.00/0

chrome oxidation with isolated proteins at low ionic strength in detergent solutions. Rosen et al. (1979, 1983) found that the oxidation of horse cytochrome *c* and *Rb. sphaeroides* cytochrome c_2 can be described by a simple equilibrium of the cytochrome in solution with a single reaction center bound state, as shown in Scheme I. The oxidation times, $\tau_c = k_c^{-1}$, for bound *Rb. sphaeroides* cytochrome c_2 and horse cytochrome *c* were found to be 1 and 20 μs, respectively (Rosen et al., 1983, 1979).

Scheme I

$$\text{cyt free} \underset{k_{-a}}{\overset{k_a}{\rightleftarrows}} \text{cyt bound} \xrightarrow{k_c} \text{cyt ox}$$

In contrast to this simple kinetic scheme, other workers (Dutton & Prince, 1978; Moser & Dutton, 1988; Overfield & Wraight, 1986; Overfield et al., 1979) found that reaction center driven cytochrome oxidation requires a three-state model, as shown in Scheme II. By analogy to the early in vivo

Scheme II

$$\text{cyt free} \underset{k_{-a}}{\overset{k_a}{\rightarrow}} (\text{distal} \underset{k_{-b}}{\overset{k_b}{\rightleftarrows}} \text{proximal}) \xrightarrow{k_c} \text{cyt ox}$$

model, the distal and proximal states both represent reaction center–cytochrome complexes, but electron transfer only occurs from the proximal state (Moser & Dutton, 1988; Overfield & Wraight, 1986; Overfield et al., 1979). In these experiments, the oxidation of *Rb. sphaeroides* cytochrome c_2 was seen to be the sum of three reactions: a diffusional second-order reaction and two first-order reactions (τ_b = 400–500 μs and τ_c = 0.6–1.5 μs). The fast component (τ_c) is attributed to electron transfer from cytochrome in a favorable or proximal configuration. The slower component (τ_b) is associated with the conversion time between distal and proximal configurations. The viscosity dependence of this slower reaction demonstrates the requirement for translational and/or rotational diffusion in the distal to proximal conversion (Moser & Dutton, 1988). These more complex in vitro kinetics reproduce the format seen in vivo and imply that an equilibrium between electron-transfer productive and nonproductive binding configurations is an inherent feature of the reaction center–cytochrome interaction. However, this conclusion is at odds with the interpretation that the multiphasic in vivo cytochrome oxidation kinetics arise from the organization of reaction centers in supercomplexes (Joliot et al., 1989; Lavergne & Joliot, 1991).

The two sets of in vitro kinetic data agree on the time constants for the fast oxidation component for each cytochrome, but they differ in the number kinetic components seen with saturating concentrations of reactants. In the two-state mechanism all of the cytochrome oxidation occurs with a single time constant with saturating amounts of cytochrome, while in a three-state mechanism two time constants are seen. In this paper we present evidence that suggests that the three-state kinetic model may not be an intrinsic feature of the reaction center–cytochrome association in vitro but may arise from differences in the physical state of the reaction center. Despite the uncertainty in the kinetic pathway for the slow oxidation components, there is uniform agreement that electrostatics play a primary role in the stabilization of the reaction center–cytochrome *c* electron-transfer complexes, as indicated by the strong ionic strength dependence for all kinetic components (Dutton et al., 1975; Moser & Dutton, 1988; Overfield & Wraight, 1986).

Two models of an electrostatically stabilized, electron-transfer complex between the *Rb. sphaeroides* reaction center and a soluble *c*-cytochrome have been built (Allen et al., 1987; Tiede et al., 1988; Tiede & Chang, 1988). These models differ in many substantial ways, including the site for cytochrome docking on the reaction center and on the orientation of the cytochrome in the complex (Tiede et al., 1988; Tiede & Chang, 1988). However, both models are based upon the premise that the reaction center–cytochrome complex is stabilized by the formation of complementary charged pairs formed between specific ionized residues on the surface of the reaction center and cytochrome proteins.

In order to gain insight into the role of the protein in the formation of transient electron-transfer complexes, we have examined the electron transfer between the *Rb. sphaeroides* R-26 reaction center and a series of structurally homologous *c*-cytochromes. In this work we show that characteristic first-order electron-transfer rates for 1:1 complexes formed at low ionic strength between the reaction center and the different *c*-cytochromes vary by a factor of almost 100, and second-order rates are found to differ by greater than 10^6. These data serve as a guide for the development of a model of the molecular recognition that leads to the formation of electrostatically stabilized reaction center–cytochrome *c* complexes. We have begun to develop a model that emphasizes the importance of electrostatic potentials on "encounter surfaces" for the reaction center and different *c*-cytochromes. A comparison of the electrostatic potential surfaces for the different *c*-cytochromes and their characteristic rates of electron transfer suggests that a primary factor in determining the configuration of a particular reaction center–cytochrome *c* complex is the structure of delocalized electrostatic potentials of the two proteins and not the location of specific charged residues.

MATERIALS AND METHODS

Preparation of Materials. Reaction centers from photosynthetically grown *Rb. sphaeroides* R-26 cells were prepared with the detergent lauryldimethylamine *N*-oxide (LDAO) as described previously (Wraight, 1979). Reaction centers were eluted from the final DEAE-Sephacel column in 0.03% LDAO, 160 mM NaCl, 10 mM Tris, and 1 mM EDTA, pH 7.8 at room temperature. Fractions with an absorbance ratio at 280/802 nm of less than 1.28 were pooled, supplemented with 1 ubiquinone-10/reaction center, and dialyzed overnight against 0.01% LDAO, 10 mM Tris, and 1 mM EDTA, pH 7.8 at 4 °C. Reaction centers were then stored frozen at −80 °C.

Cytochromes c_2 from *Rhodobacter capsulatus*, *Rhodopseudomonas viridis*, and *Rb. sphaeroides* were isolated essentially as described previously (Bartsch, 1978). Cytochromes *c* from tuna, horse, *Saccharomyces cerevisiae*, *Candida krusei*, and *Pseudomonas aeruginosa* were obtained from Sigma and were used without further purification. Extinction coefficients of 30.8 and 27.6 mM^{-1} cm^{-1} were used for the cytochromes c_2 and *c*, respectively.

Assay of Electron-Transfer Rates. Single-turnover, laser-flash-induced electron-transfer rates from the ferroheme to the photooxidized reaction center were measured in 0.01% LDAO, 10 mM Tris, and 1 mM EDTA, pH 7.8, with a reaction center concentration of 1 μM. In addition to a variable amount of cytochrome, the reaction mixture contained 20 μM 2-hydroxy-1,4-naphthoquinone, 10 μM phenazine methosul-

fate, and 10 μM ubiquinone-0 as redox mediators. The redox potential was set at approximately +100 mV by additions of dithionite in an argon-purged 1-cm path-length cuvette.

The kinetics of electron transfer were routinely measured by monitoring the single-beam absorbance transients associated with the reduction of the flash-induced P^+ at 860 nm. Corroborative measurements were also made by monitoring the disappearance of the P^+ 1250-nm band and by monitoring the kinetics of cytochrome oxidation by recording the 550-nm − 540-nm difference absorbance transients. All three measurements gave equivalent results. The flash excitation was a 590-nm, 20 nm wide, 1.5 mJ/cm^2 laser pulse provided by YAG (Molectron) pumped rhodamine dye laser. The CW probe beam was shuttered to open 50 ms before the laser excitation, and the shutter closed immediately after each single-beam transient was recorded. Four to eight transients were averaged at a single wavelength, with 20 s between recordings. There were no discernible differences between the individual transients. The detector was a silicone avalanche photodiode (EG&G) that provides a response time of less than 0.1 μs.

The absorbance transients were fit to the sum of one to three single exponentials, using a Levenberg–Marquardt nonlinear least squares fitting routine (Dr. Seth Snyder, ANL). These were unrestricted fits for the amplitudes and reaction times. The initial guess values were systematically changed to ensure that the solutions did not correspond to local minima.

Electrostatic Calculations. Electrostatic potential maps for the *c*-cytochromes and the reaction center were calculated from the X-ray crystal structures using the program DelPhi. The program calculates the electrostatic potential throughout a volume that includes a protein using a linearized form of the Poisson–Boltzmann equation (Gilson & Honig, 1988; Gilson et al., 1985; Nicholls & Honig, 1991). The coordinates for the tuna (Takano & Dickerson, 1981), *Rhodospirillum rubrum* (Bhatia, 1981; Salemme et al., 1973), and *P. aeruginosa* (Matsuura et al., 1982) cytochromes were obtained from the Brookhaven Protein Data Bank (Abola et al., 1987; Bernstein et al., 1977), files 5cyt/pdb, 3c2c.pdb, and 451c.pdb, respectively. The coordinates of the horse heart (Bushnell et al., 1990) and yeast iso-1 (Louie & Brayer, 1990; Louie et al., 1988) cytochromes *c* were provided by Prof. G. Brayer (University of British Columbia). The coordinates of the *Rb. capsulatus* cytochrome c_2 (Holden et al., 1987) were provided by Prof. H. Holden (University of Wisconsin, Madison). Cytochromes c_2 have been crystallized from *Rb. sphaeroides* (Allen, 1988) and *R. viridis* (Miki et al., 1986), but the structures are not yet available. In lieu of these structures, models were built from homologous cytochrome structures. A model of the *Rb. sphaeroides* cytochrome c_2 (Tiede et al., 1988; Tiede & Chang, 1988), was built by modifying the structure of the cytochrome c_2 from *Paracoccus denitrificans* (Ambler et al., 1981; Timkovich & Dickerson, 1976). The model cytochrome was built by replacing the charged amino acid side chains on the *P. denitrificans* protein with residues corresponding to the *Rb. sphaeroides* sequence. This required 33 changes plus deletion of seven residues from the C-terminus. Before the *Rb. capsulatus* structure became available, the *P. denitrificans* structure was the most closely homologous to the *Rb. sphaeroides* cytochrome c_2 (Meyer & Kamen, 1982). This model of the *Rb. sphaeroides* cytochrome c_2 was used in the electrostatic calculations described below. Similarly, a model of the *Rps. viridis* cytochrome was built from the tuma structure, requiring 20 side-chain replacements, plus the addition of five residues to the C-terminus. In both models, only the ionized side chains were altered to match those of the target sequence using the program BIOGRAF. The peptide backbones of the parent structures were not altered. The new residues were positioned to give a compact structure, without making contacts with other residues in the structure. These model structures were used in an attempt to estimate the electrostatic consequences of the different distributions of charged residues in the *Rb. sphaeroides* and *Rps. viridis* sequences.

Procedures for the calculation of electrostatic potential throughout a volume that includes a protein have been described in detail (Gilson & Honig, 1988; Gilson et al., 1985; Gunner & Honig, 1991; Nicholls & Honig, 1991). A dielectric constant of 80 was assigned to the water-accessible regions, and a dielectric constant of 4 was assigned to the protein interior (Harvey, 1989). Water-accessible regions were defined by tracing the protein with a 1.4-Å-radius probe molecule. The calculations included an ionic strength of 20 mM and a Stern layer (electrolyte exclusion zone) of 2 Å.

An "encounter surface" was simulated for each protein by a Connelly surface that was calculated by tracing the structure with a 5-Å-radius probe. This surface, rather than one defined by the atomic van der Waals radii, was used to model an encounter surface for two reasons. First, the 5-Å Connelly was used to approximate a more typical distance of closest approach in a simple reaction center–cytochrome collision that does not involve the rearrangement of protein side chains. In docking two protein structures without the mutual rearrangement of protein side chains, the large size of these macromolecules only allows one or a very small number of residues to be in van der Waals contact. There are substantial regions on the van der Waals surface which are not accessible to the companion protein, without mutual rearrangement of the protein side chains. The 5-Å Connelly surface, rather than the van der Waals surface, was used to test for likely regions of strong electrostatic potential in bimolecular complexes that do not depend upon specific charge pairing or mutual rearrangement of side chains. Second, electrostatic potentials on the 5-Å Connelly surface were found to be less sensitive to the exact positions of the amino acid side chains than a surface generated with the atomic van der Waals radii. Uncertainty in side-chain position is clearly a feature of the model *Rb. sphaeroides* and *Rps. viridis* cytochrome structures. In addition, side-chain location is frequently uncertain in measured crystal structures due to motional averaging. The assay of electrostatic potentials on the 5-Å Connelly surface allows the electrostatic properties of the different cytochromes to be compared, even though the side-chain positions are not uniformly known.

The electrostatic calculations were done with two atom charge sets. One included only the terminal nitrogen and oxygen atoms of lysine, arginine, aspartate, and glutamate residues, the N- and C-terminal atoms, and the heme atoms (Northrup et al., 1981). The other charge set assigned partial charges to all protein (CHARMM20), heme (Northrup et al., 1981), and reaction center pigment (Gunner & Honig, 1991) atoms. Protons were added to the structures as described previously (Gunner & Honig, 1991). The resulting electrostatic potential maps on the encounter surfaces calculated with the full and partial charge sets did not differ in gross features of the electrostatic potential maps but differed mainly in the level of detail detected in the contours.

Dipole moments, $\mu_D = \sum q_i r_i$, were calculated for each cytochrome, where q_i and r_i represent the charge and position of the *i*th atom with respect to the center of mass (Dixon et al., 1989; Koppenol & Margoliash, 1982; Northrup et al.,

Table I: Electron-Transfer Rates between the *Rb. sphaeroides* Reaction Center and a Series of *c*-Cytochromes

		cytochrome-independent kinetic compounds					cytochrome-dependent kinetic compounds
cytochrome	redox[a] (mV)	τ_1[b] (μs)	A_1[c]	τ_2[b] (μs)	A_1[c]	K_D (μM)	k_2 (M^{-1} s^{-1})
sphaeroides	350	0.7(0.2)	0.9	2(1)	0.1	1–3	$2(1) \times 10^9$
capsulatus	365	0.5(0.2)	0.9	3(2)	0.1	4–6	$8(2) \times 10^8$
tuna	260	0.7(0.2)	0.6	12(2)	0.4	0.5–1	$2(1) \times 10^9$
horse	260	1.0(0.2)	0.3	23(4)	0.7	1–4	$1(1) \times 10^9$
cerevisiae	260		0.0	40(5)	1.0	0.4–1.4	$4(1) \times 10^8$
krusei	265		0.0	44(5)	1.0	0.7–1.2	
rubrum	324		0.0		0.0		2×10^8 [d]
viridis	300		0.0		0.0		$6(1) \times 10^7$
aeruginosa	270		0.0		0.0		$<10^3$

[a] $E_h(P/P^+)$ = 450 mV. [b] Lifetimes of the first-order kinetic components. The numbers in parentheses are the standard deviation of lifetimes determined by curve-fitting absorbance transients measured in titrations with varying cytochrome concentration. [c] Relative amplitudes of first-order components in the fast-phase kinetics. The absolute amplitudes of the fast-phase components varied in titrations with different reaction center samples as indicated in Figure 2 and in the text, but the number of kinetic components resolved in the fast kinetic phase and their lifetimes and amplitudes with respect each other were found to be constant. The amplitudes in this table reflect the relative contribution to the fast-phase kinetics. [d] Long et al., 1989.

1986). In addition, positive $\mu_+ = \sum q_+ r_i$ and negative $\mu_- = \sum q_- r_i$ charge moments were calculated using only the positively and negatively charged atoms, respectively. These charge moments provide a measure of anisotropy in the distribution of positive and negative charges with respect to the center of mass. For example, the vector sum of the atom positions will be zero for a uniform charge distribution, yielding a null moment. In contrast, the moment will be large if the charged atoms are clustered in one portion of the molecule. The magnitude of the charge moment, normalized for total positive or negative charge, $|\mu_+|/\sum q_+$ or $|\mu_-|/\sum q_-$, provides a parameter for charge anisotropy that is independent of the total number of charged atoms. The normalized charge moments have been used to compare extents of charge clustering in the different cytochromes.

RESULTS

Electron-Transfer Characterization

The kinetics for electron transfer from the ferrocytochromes to the photooxidized *Rb. sphaeroides* reaction center at low ionic strength were examined as a function of cytochrome concentration for eight cytochromes. The reaction center concentration was 1 μM in each experiment. The optical transients were fit as the sum of one to three single-exponential components. The amplitudes and lifetimes of the kinetic components at each cytochrome concentration were allowed to vary without restriction. A comparison of the time constants as a function of cytochrome concentration allowed the kinetic components to be classified as having reaction times that were either independent or dependent upon cytochrome concentration. The kinetic components whose rates were independent of cytochrome concentration identified first-order electron-transfer reactions associated with reaction center–cytochrome complexes existing before the laser flash. The kinetic components whose rates changed with different cytochrome concentrations identified higher order kinetic processes. In general, the electron transfer from the ferrocytochrome to photooxidized reaction center was found to be the sum of both first- and second-order kinetic components. However, each cytochrome could be associated with a characteristic set of rate constants and kinetic components. Table I summarizes the characteristic kinetic parameters found for the different cytochromes. The cytochromes are listed in decreasing order of electron-transfer efficacy with the reaction center. Representative kinetics are shown in Figure 1. To a variable extent (0%–10%), a slow component with a reaction time in the millisecond time range was seen in the reduction kinetics for P^+ with all cytochromes. When present, the amplitude and rate constant of this minor component did not appear to depend upon cytochrome concentration. This kinetic component is not included in the descriptions below and, as discussed later, is assumed to reflect a fraction at the reaction center population that is not capable of forming rapid electron-transfer complexes with the soluble *c*-cytochromes.

Oxidation Kinetics with Rb. sphaeroides Cytochrome c_2. P^+ reduction kinetics as a function of *Rb. sphaeroides* cytochrome c_2 concentration are shown in Figure 1A. Strongly multiphasic kinetics are seen. Residuals to fits of the reduction transient with 5 μM cytochrome and 1 μM reaction center with two (middle) and three (bottom) components are shown in the lower portion of the figure. The three-component fit can be seen to be marginally better. This was consistently seen in the kinetics at all cytochrome c_2 concentrations. The three-component model fit the fast phase as the sum of two components, with reaction times of 0.7 and 2 μs in an approximate 9 to 1 relative amplitude ratio, respectively, at each cytochrome concentration. The independence of the reaction times for these two fast components identifies them as first-order kinetic processes that are associated with reaction center–cytochrome complexes existing before the photooxidation of the reaction center. The increase in the amplitudes of these fast-phase components with respect to the slow phase reflects a shift in the binding equilibrium toward the bound state as the cytochrome concentration increased. These results are compatible with previous work that has described the first-order kinetic response as a single exponential, with a reaction time of 0.6–1.4 μs (Long et al., 1989; Overfield et al., 1979; Rosen et al., 1983).

In contrast to the relatively consistent kinetic description of the fast, first-order component, there has been considerable variation in the kinetic model and rate constants reported in the literature for the slower kinetic phase. In general, the reaction rate of the slow component is seen to increase with increasing cytochrome concentration. At low cytochrome and reaction center concentrations, this slow component displays a linear dependence on cytochrome concentration reflecting a collisional rate process. Second-order rate constants are reported in the range 1.5×10^8–8×10^8 M^{-1} s^{-1}. In many (Long et al., 1989; Moser & Dutton, 1988; Overfield et al., 1979) but not all cases (Rosen et al., 1983, 1979), this second-order process has been seen to reach a pseudo-first-order limit, with the limiting reaction time reported in the range of 65–600 μs (Long et al., 1989; Moser & Dutton, 1988; Overfield

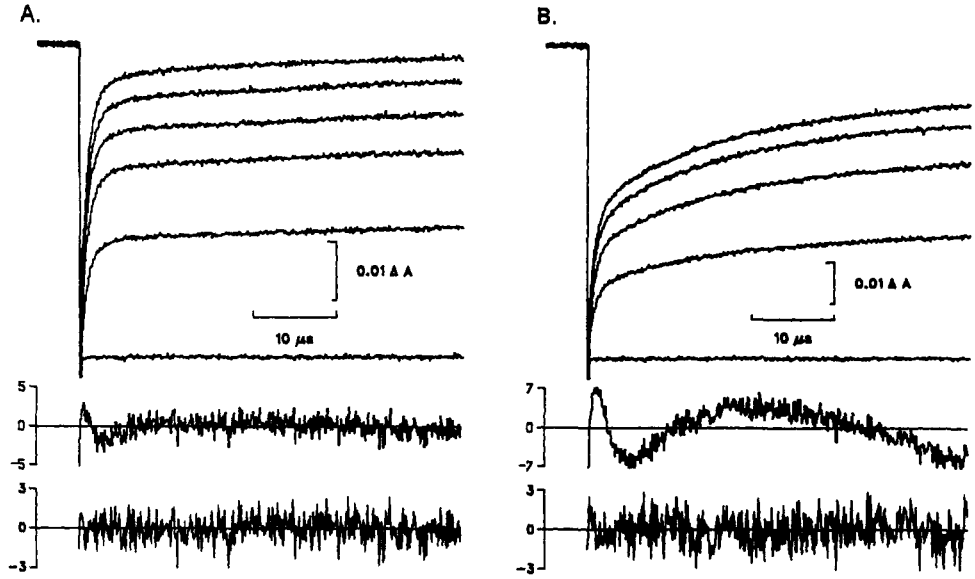

FIGURE 1: Reduction kinetics for P^+, measured at 860 nm as a function of cytochrome concentration. Part A shows the transients measured in the presence of 0 and then 1–10 μM *Rb. sphaeroides* cytochrome c_2. The lower two individual traces are the residuals from fitting the absorbance transient measured with 5 μM cytochrome as the sum of two and three exponential components. The amplitudes and lifetimes of the components in the two-component fit were $A_1 = -3.73 \times 10^{-2}$, $\tau_1 = 1.0$ μs and $A_2 = -1.00 \times 10^{-2}$, $\tau_2 = 92$ μs. The parameters in the three-component fit were $A_1 = -3.35 \times 10^{-2}$, $\tau_1 = 0.7$ μs, $A_2 = -0.72 \times 10^{-2}$, $\tau_2 = 2.2$ μs, and $A_3 = -0.97 \times 10^{-2}$, $\tau_3 = 102$ μs. Part B shows the absorbance transients in the presence of 0 and then 1–10 μM tuna cytochrome *c*. The lower two individual traces are the residuals from fitting the absorbance transient measured with 5 μM cytochrome as the sum of two and three exponential components. The amplitudes and lifetimes of the components in the two-component fit were $A_1 = -2.39 \times 10^{-2}$, $\tau_1 = 1.7$ μs and $A_2 = -2.64 \times 10^{-2}$, $\tau_2 = 42$ μs. The parameters in the three-component fit were $A_1 = -2.61 \times 10^{-2}$, $\tau_1 = 0.8$ μs, $A_2 = -1.92 \times 10^{-2}$, $\tau_2 = 14$ μs, and $A_3 = -1.28 \times 10^{-2}$, $\tau_3 = 143$ μs. Both samples contained 1 μM reaction center, 0.03% LDAO, 10 mM Tris and 1 mM EDTA, plus redox mediators as described under Materials and Methods. The samples were posed at a reduction potential of 100 mV in an argon-purged, anaerobic 1-cm path-length cuvette.

et al., 1979). The percentage of the cytochrome oxidation proceeding by the pseudo-first-order pathway was reported to be either 26% (Long et al., 1989) or 50% (Mosher & Dutton, 1988; Overfield et al., 1979).

In this work we have reproduced several of the different kinetic formats reported in the literature. An illustration is shown in Figure 2A, with a Scatchard plot of two titrations of the reaction center with *Rb. sphaeroides* cytochrome c_2. The fraction of reaction centers with bound cytochrome c_2 was defined as the sum of both first-order components. The two experiments differed only in the reaction center batch, which were identical as far as could be determined by SDS–PAGE, ion-exchange chromatography, and optical absorption assays of protein purity, and both reaction center preparations exhibited equivalent photochemical oxidation and recovery kinetics in the absence of added cytochrome. The same cytochrome c_2 batch was used in both experiments, and all other conditions (0.03% lauryldimethylamine *N*-oxide, 10 mM Tris, 1 mM EDTA, pH 7.8) were as equivalent as possible. The reaction times and relative extents of the two fast components were equivalent in the two titrations, as described above. However, the experimentally determined disassociation constant and extent of the fast kinetic phases differed. In one experiment (marked by circles, Figure 2A) the fast phases showed a dissociation constant of 0.9 μM, with 1 cytochrome binding site per reaction center. The concentration dependence of the rate constant for the slow kinetic phase in this titration fits a second-order dependence ($k_a = 2 \times 10^9$ M^{-1} s^{-1}) throughout the cytochrome concentration range (Figure 3A). In this experiment, all of the cytochrome oxidation can be explained by a simple equilibrium between reaction center–cytochrome complexes that give rise to first-order kinetics and free states that show a collisional reaction without approaching a pseudo-first-order limit at high cytochrome concentration. The presence of two first-order components in the fast phase suggests a modified form of the two-state kinetic model, in which free cytochrome is in equilibrium with two different forms of the reaction center–cytochrome complex, each associated with the different electron-transfer time constant.

In the titration with the second reaction center sample, shown by the squares in Figure 2A, the rate and ratio of the fast kinetic components are unchanged. However, the first-order kinetic components bind more weakly, exhibiting a disassociation constant of 2.2 μM, and extrapolate to a reduced stoichiometry of 0.8 site per reaction center with saturating cytochrome concentration. The remainder of cytochrome oxidation occurs through the slower kinetic pathway. The reaction rate of the slow phase deviates from a linear dependence upon cytochrome concentration that passes through the origin as expected for a second-order reaction (Figure 3A). A double-reciprocal plot of these data (Figure 4) shows that the slow kinetic component for this second experiment can be described by Michaelis–Menten kinetics with a limiting reaction time, $1/V_m$, of about 55 μs and a Michaelis constant, K_M, of 20 μM. This behavior differs markedly from the slow kinetic component detected in the first experiment. This set of data is consistent with the three-state model described above (Dutton & Prince, 1978; Moser & Dutton, 1988; Overfield & Wraight, 1986; Overfield et al., 1979), in which the bound cytochrome is distributed between kinetically competent, proximal, and incompetent, distal, configurations. In terms of the previously defined model (Dutton & Prince, 1978; Moser & Dutton, 1988; Overfield & Wraight, 1986; Overfield et al., 1979), the data in Figure 4 suggest that the reaction time for the distal to proximal conversion is about 55 μs ($k_c = 1.8 \times 10^4$ s^{-1}). This is consistent with a 65-μs component reported in one set of data (Long et al., 1989) but is considerably shorter than the 500–600-μs reaction time reported in other sets (Moser & Dutton, 1988; Overfield et al., 1979).

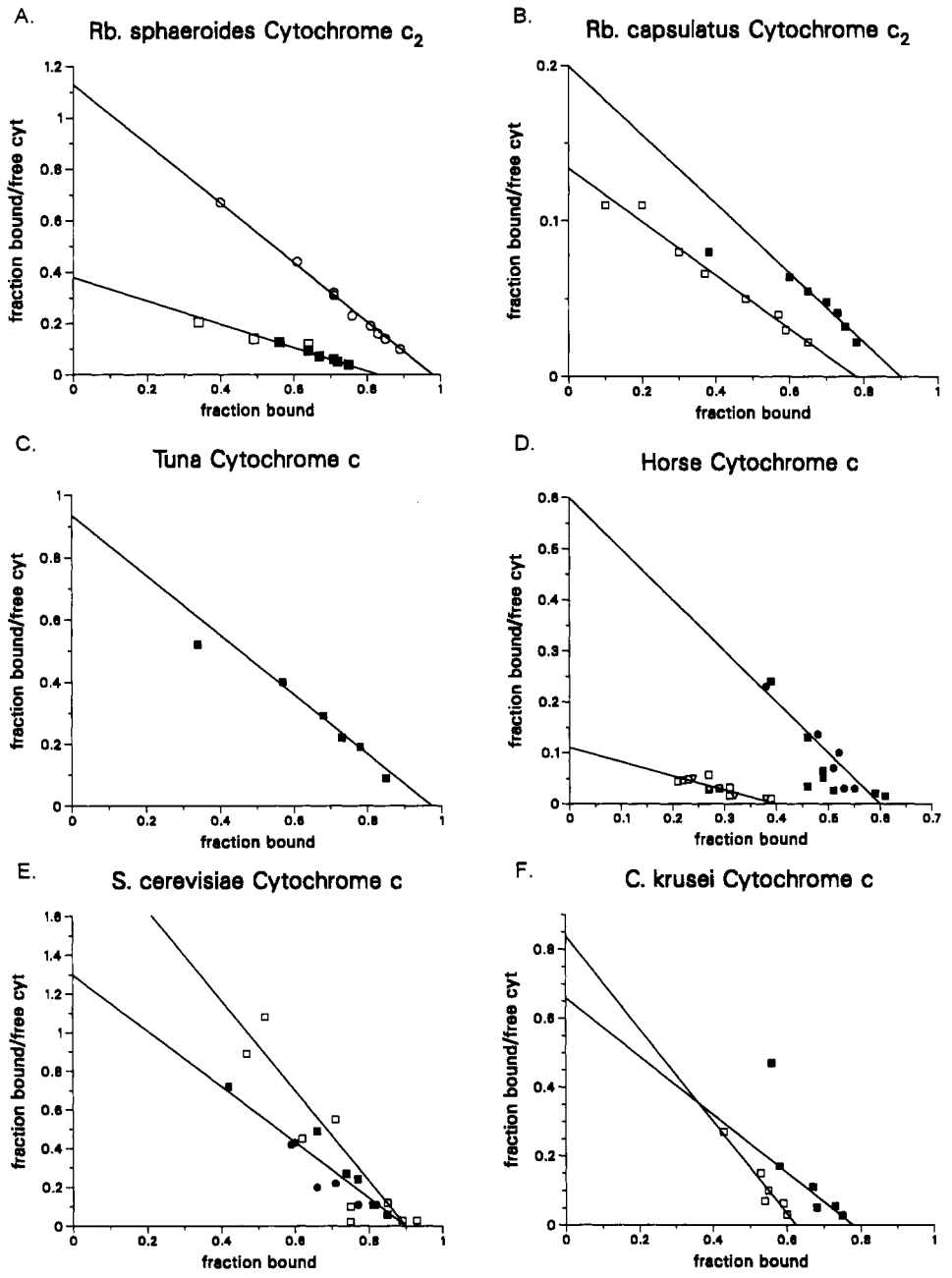

FIGURE 2: Scatchard plots of cytochrome binding to the *Rb. sphaeroides* reaction center. Cytochrome titrations with respect to the fixed reaction center concentration of 1 μM were carried out as shown in Figure 1. Independent fits to the electron-transfer kinetics as a function of cytochrome concentration identified first-order kinetic components with reaction times that remained constant throughout the titration. The fraction of bound cytochrome at a specific cytochrome concentration was identified by the relative extent of the cytochrome oxidation proceeding with first-order kinetics. The different symbols mark titrations with different reaction center samples. Other conditions were as described in Figure 1 and in the text. Representative lines are drawn through the data, and the corresponding binding constants are shown in the figure. Part A shows titrations with *Rb. sphaeroides* cytochrome c_2. The axes intercepts for the line drawn through the data marked with circles correspond to a disassociation constant, K_D, of 0.9 μM and a stoichiometry, n, of 0.98 site per reaction center. The line drawn through the data marked with squares corresponds to a K_D of 2.2 μM and $n = 0.83$. Part B shows titrations with *Rb. capsulatus* cytochrome c_2. The line drawn through the filled squares corresponds to a K_D of 4.5 μM and $n = 0.9$. The line through the open squares corresponds to a K_D of 5.8 μM and $n = 0.78$. Part C shows titrations with tuna cytochrome c. The line corresponds to a K_D of 1 μM and $n = 0.97$. Part D shows titrations with horse heart cytochrome c. Lines corresponding to $K_D = 1$ μM, $n = 0.6$ and $K_D = 3.6$ μM, $n = 0.4$ are drawn through the data marked with filled and open symbols, respectively. Part E shows titrations with *S. cerevisiae* cytochrome c. Lines with $K_D = 1.4$ μM, $n = 0.9$ and $K_D = 0.4$ μM, $n = 0.9$ are drawn through the data. Part F shows titrations with *C. krusei* cytochrome c. Lines with $K_D = 1.2$ μM, $n = 0.78$ and $K_D = 0.7$ μM, $n = 0.63$ are drawn through the data. Cytochrome titrations measured with different reaction center samples are indicated with different symbols. In each case, the experimental conditions were as identical as possible.

Differences in the maximal extent of the fast kinetic components were seen for other cytochromes, also suggesting variations between simple two-state and three-state kinetic models. One possible explanation is that the electron-transfer incompetent mode of binding is not an intrinsic feature of the *Rb. sphaeroides* reaction center–cytochrome c_2 interaction but rather is a function of a variable feature of the reaction center, possibly its aggregation number. This possibility is discussed later.

In contrast to the variation seen in the behavior of the slow kinetic component, both in this work and in the comparison of literature reports, it is important to emphasize that the reaction times measured for the rapid, first-order cytochrome oxidation components were the same for all reaction center

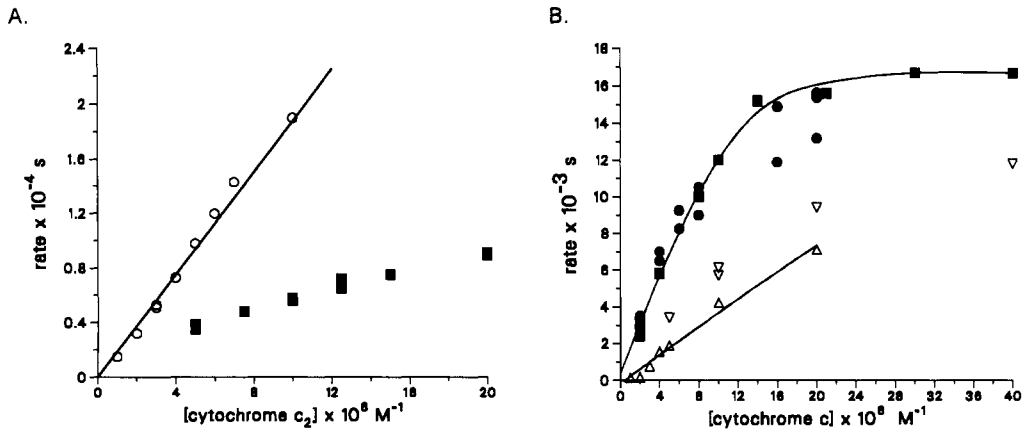

FIGURE 3: Plots of the rate of the cytochrome concentration dependent kinetic component versus cytochrome concentration. Part A shows the *Rb. sphaeroides* cytochrome c_2 dependent kinetic components measured with two different reaction center samples. One titration, marked by the circles, shows a linear dependence corresponding to a second-order rate constant of 2×10^9 M^{-1} s^{-1}. The accompanying first-order components are shown by the titration marked with circles in Figure 2A. The second titration, marked by the filled squares, does not show the expected linear dependence that passes through the origin as expected for a second-order kinetic process. The same data are shown plotted in a double-reciprocal plot, indicated by the unfilled squares in Figure 4. The first-order components accompanying these slow kinetic components are shown by the squares in Figure 2A. Part B shows the concentration dependence in the rate of the slow kinetic component for other cytochromes. Three separate titrations with horse cytochrome *c*, using different reaction center preparations, are marked by filled circles, filled squares, and inverted triangles. The same data are shown in a double-reciprocal plot in Figure 4 using the same symbols. The corresponding Scatchard plot for the fast-phase components is shown in Figure 2D using the same symbols. The triangles mark a titration for *S. cerevisiae* cytochrome *c*.

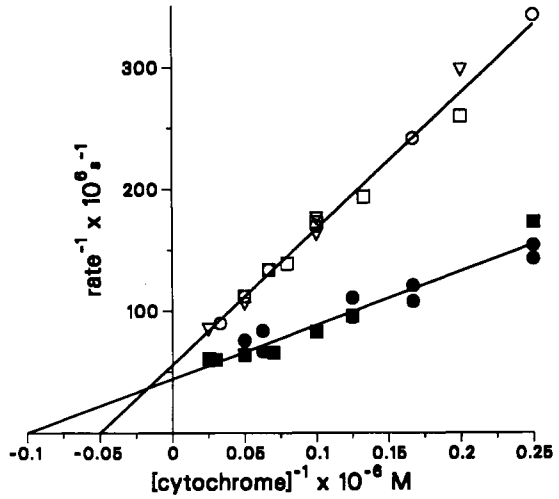

FIGURE 4: Double-reciprocal plots of the slow, cytochrome-dependent kinetic components. The squares mark the plot for *Rb. sphaeroides* cytochrome c_2. These slow kinetic components were accompanied by the fast, first-order components marked by the filled sqaures in Figure 2A. The circles mark a plot of the slow-phase kinetics for *Rb. capsulatus* cytochrome c_2. The binding behavior for the accompanying fast-phase components is shown in Figure 2A, marked with the unfilled squares. The filled squares, filled circles, and inverted triangles mark titrations with horse cytochrome *c* using different reaction center samples. These data were also plotted in Figure 3B using the same symbols, and the corresponding plots for the fast-phase components are shown in Figure 2D, marked with the same symbols. The line drawn through the unfilled symbols corresponds to a V_m^{-1} of 56 μs and K_M of 20 μM. The line drawn through the filled symbols corresponds to a V_m^{-1} of 44 μs and K_M of 10 μM.

preparations. This suggests that these kinetic parameters are intrinsic, characteristic features of the *Rb. sphaeroides* reaction center–cytochrome c_2 interaction. As a result, these fast kinetic components will be the focus of the ensuing comparison between the electron-transfer characteristics of the different *c*-cytochromes and their electrostatic properties.

Other Cytochromes with Predominately Submicrosecond Oxidation Kinetics. The electron transfer between the *Rb. sphaeroides* reaction center and the *Rb. capsulatus* cytochrome c_2 was found to closely parallel the kinetics recorded for the *Rb. sphaeroides* cytochrome. The time constant of the fastest first-order component was detected to be marginally faster than with the *Rb. sphaeroides* cytochrome. A small contribution from a slower first-order component was also detected with a reaction time of about 3 μs, slightly slower than with the *Rb. sphaeroides* cytochrome. The kinetic pattern is similar to that seen with the *Rb. sphaeroides* cytochrome, suggesting that both cytochromes form similar complexes with the reaction center. Fast first-order components were not detected in a recent study of the electron transfer between the *Rb. capsulatus* cytochrome and the *Rb. sphaeroides* reaction center (Caffrey et al., 1992), presumably because these kinetics are faster than the >1-μs time response used in this previous work. Scatchard plots of *Rb. capsulatus* cytochrome c_2 also showed the disassociation constant for the first-order components to vary with different reaction center preparations in the range 4–6 μM (Figure 2B), with the maximum extent of first-order stoichiometry varying between 0.78 and 0.9 site per reaction center. In the titration in which the maximum extent of the fast, first-order components extrapolated to 0.78 site per reaction center, the slow kinetic phase could be resolved to reach a pseudo-first-order reaction time limit of about 55 μs, shown in Figure 4. A linear dependence of electron-transfer rates for the slow phase at low cytochrome concentrations suggested a second-order rate constant of about 8×10^8 M^{-1} s^{-1}.

The electron-transfer kinetics with tuna cytochrome *c* are shown in Figure 1B. The residuals clearly show that if the data are to be fit as the sum of single exponentials, then at least three components are needed. The two fastest components in the fits had lifetimes of 0.7 and 12 μs with amplitudes that corresponded to 60% and 40%, respectively, of the total first-order absorbance change. Both the lifetimes and relative amplitudes of these two components were found to be approximately constant during the titration with tuna cytochrome. The fast oxidation phase of the tuna cytochrome *c* differs from those of the *Rhodobacter* cytochromes c_2 by having two first-order components of nearly equal amplitude. While the extents of these components with respect to each other remained constant during the titration with changing cyto-

chrome concentration, Scatchard plots indicate that their sum accounts for 1 binding site per reaction center. These data also are supportive of a simple, two-state kinetic model with no (10% or less) second-order component reaching a pseudo-first-order limit. However, these data show the tuna cytochrome to form at least two kinetically distinguishable complexes with the reaction center. One mode of tuna cytochrome *c* binding to the reaction center appears to yield electron-transfer rates comparable to those of the major first-order component with the *Rb. sphaeroides* and *Rb. capsulatus* cytochromes, while the second mode yields a reaction time approximately 17 times slower and is close to the next three cytochromes listed in Table I.

Cytochromes with Predominately Tens of Microseconds Oxidation Kinetics. The reaction time for the predominant first-order kinetic component for the horse, *S. cerevisiae*, and *C. krusei* cytochromes *c* was found to be on the tens of microseconds time scale. For horse cytochrome *c* this predominant first-order component was found to have a reaction time of 23 μs that represented 70% of the first-order kinetic change. A faster first-order kinetic component was also indicated with a 1-μs reaction time, that comprised the remaining 30% of the first-order kinetic response. The reaction time for the major component is in good agreement with previous work that describes the first-order kinetics as a single component measured with 3 μM reaction center concentration (Rosen et al., 1983). More recent curve-fitting techniques have also found that the first-order oxidation kinetics of horse cytochrome *c* are better fit as the sum of two exponentials (Long et al., 1989), although in this case the fit gave nearly equal contributions of components with reaction times of 9 and 55 μs. These differ from the kinetic components obtained here. However, it may be significant to note that these latter experiments (Long et al., 1989) used a 10-fold higher reaction center concentration (10 μM). It is not clear whether the kinetic differences arise from the different experimental conditions or whether the differences result from different fitting procedures. However, the difference in reaction center concentrations used in these experiments may be significant in light of the possible aggregation state dependence of the slow-phase cytochrome kinetics discussed below.

Unlike the other cytochromes listed in Table I, the amplitude of the fast, first-order oxidation phase for horse cytochrome *c* was seen to extrapolate to significantly less than 1 site per reaction center in Scatchard plots for all reaction center preparations (Figure 2). The stoichiometry varied from 0.4 to 0.75 site per reaction center in different experiments, with the dissociation constant varying in the range 1–5 μM. In these titrations, the slow kinetic component reached a pseudo-first-order limit, with a reaction time of 44–55 μs (Figures 3B and 4). Thus, the in vitro kinetics for horse cytochrome *c* appear to require a three-state model unlike the other cytochromes. However, like the other cytochromes, the variation in the extent and reaction times of the slow kinetic component with different reaction center preparations suggests that these kinetic properties are not necessarily characteristic features of the horse cytochrome *c* interaction with the reaction center. This conclusion is reenforced by noting that the double-reciprocal plots show that the slow kinetic phase for one titration with horse cytochrome *c* matches those with *Rb. sphaeroides* and *Rb. capsulatus* cytochromes c_2 (Figure 4).

The oxidation of cytochromes *c* from *S. cerevisiae* and *C. krusei* differed from the others in that the fast oxidation phase was adequately described by a single first-order kinetic component. The oxidation time found for both cytochromes was about 40 μs. Faster kinetic components were not seen. A reaction time of 20 μs was reported for the fast-phase component of yeast cytochrome *c* (Long et al., 1989).

Considerable variation was seen in the relative extents of the fast, concentration-independent and slower, cytochrome-dependent kinetic components. For example, for the *C. krusei* cytochrome *c* the stoichiometry of first-order binding sites varied in the range of 0.6 to 0.8 per reaction center, with corresponding dissociation constants of 0.7 μM and 1.2 μM, respectively (Figure 2). The titrations with the *S. cerevisiae* cytochrome *c* showed considerable scatter in the relative extents of the fast and slow kinetic components. Representative lines through the data reflect disassociation constants of 0.4 μM and 1.4 μM with 0.9 binding site per reaction center.

The slow phase of the *S. cerevisiae* cytochrome *c* oxidation exhibited a linear dependence on cytochrome concentration, reflecting a second-order rate constant of about 4×10^8 M^{-1} s^{-1} (Figure 3B). The absence of a pseudo-first-order limit to the slow oxidation phase is consistent with the binding assays that show that the stoichiometry of binding sites for the fast kinetic phase is close to 1 per reaction center. The kinetic data for the *S. cerevisiae* cytochrome *c* suggest a simple two-state kinetic mechanism. In contrast, the slow oxidation phase of the *C. krusei* cytochrome did not exhibit a linear dependence on cytochrome concentration with the 1 μM reaction center concentration used in these assays. This behavior suggests that the slow oxidation phase occurs from a distal site having an disassociation constant comparable to 1 μM. With increasing cytochrome concentration the slow phase appeared to reach a limit with reaction times in the range 200–600 μs. The existence of a pseudo-first-order limit to the slow-phase *C. krusei* oxidation is consistent with the binding assays that show that the stoichiometry for the fast, first-order oxidation phase is significantly less than 1 site per reaction center. Like the horse cytochrome *c*, the *C. krusei* cytochrome appears to require a three-state kinetic model, although, again, the relative extent of the pseudo-first-order component showed considerable variation in different experiments.

Cytochromes with No First-Order Oxidation Kinetics. The last three cytochromes in Table I show no first-order component in the electron-transfer kinetics. The electron-transfer kinetics between the *Rs. rubrum* cytochrome c_2 and the *Rb. sphaeroides* reaction center were not measured here, but previous work showed that the reaction occurs exclusively by a second-order process with a rate constant of 2.4×10^8 M^{-1} at low ionic strength (Long et al., 1989). Our results for the *Rps. viridis* cytochrome c_2 are similar. We find that the electron transfer from the *Rps. viridis* cytochrome c_2 to the reaction center occurs exclusively by a second order mechanism, with a rate constant of approximately 6×10^7 M^{-1} s^{-1}.

Finally, no electron transfer could be detected during the lifetime of P^+ (approximately 1 s) with concentrations up to 75 μM cytochrome *c*-551 from *P. aeruginosa*. The absence of even a collisional electron transfer is surprising since this cytochrome is the smallest cytochrome with the largest access to the heme edge (Meyer & Kamen, 1982).

Electrostatic Characterization

For all the cytochromes examined, the redox driving force for the ferrocytochrome to P^+ electron transfer is relatively small (100–200 mV). There is no correlation between this driving force and the characteristic electron-transfer rate. This suggests that the different first-order electron-transfer times for the cytochromes listed in Table I are likely to arise from differences in the structure of 1:1 reaction center–cytochrome

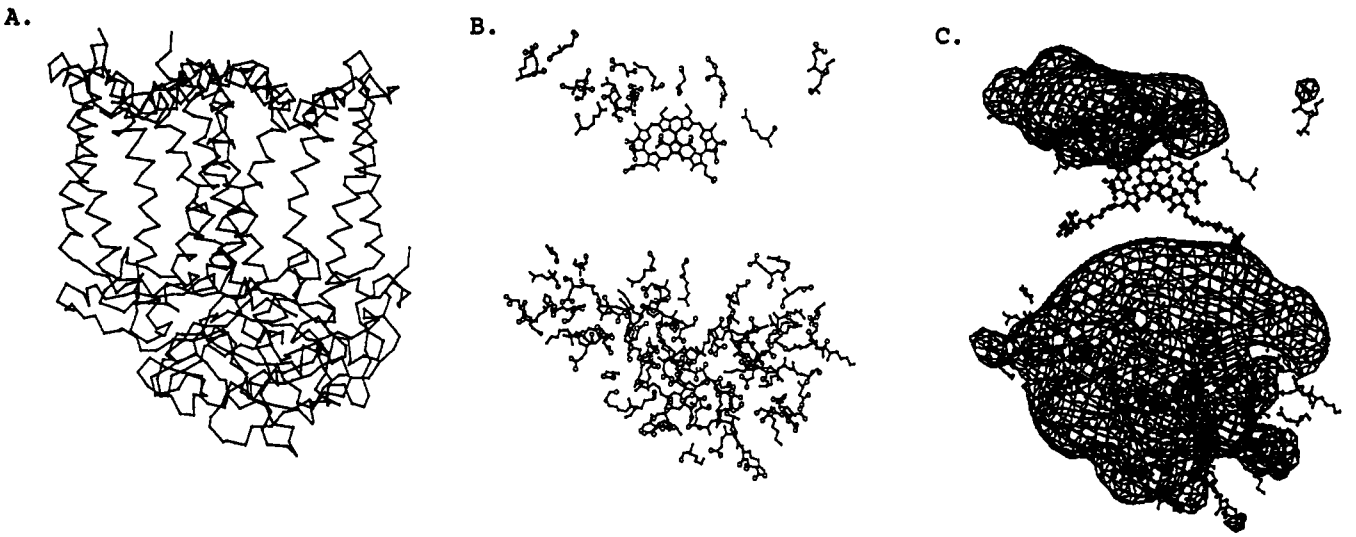

FIGURE 5: Structure of the *Rb. sphaeroides* R-26 reaction center. Part A shows the α-carbon backbone. The vertical helix on the far right is the A-helix of the L-subunit, and the A-helix of the M-subunit is on the left [see Allen et al. (1986, 1987), Chang et al., (1991), Deisenhofer and Michel (1989), El-Kabbani et al. (1991), Tiede et al. (1988), and Yeates et al. (1987) for nomenclature]. The single transmembrane helix of the H-subunit is in the front center of the structure. The approximate 2-fold symmetry axis of the reaction center is vertical. More detailed discussions of this view of the reaction center can be found in Allen et al. (1986, 1987), Chang et al. (1991), Deisenhofer and Michel (1989), El-Kabbani et al. (1991), Tiede et al. (1988), and Yeates et al. (1987). The reaction center (10^5 MW) has approximate dimensions of 40 Å × 70 Å × 75 Å. The relative size of the reaction center compared to the water-soluble *c*-cytochromes can be seen in docking models (Allen et al., 1987; Tiede et al., 1988; Tiede & Chang, 1988). Part B shows the positions of the nominally ionized lysine, arginine, glutamate, and aspartate residues and the bacteriochlorophyll dimer with the reaction center oriented as in part A. Part C shows the calculated –3 kT isopotential energy surface along with the bacteriochlorophyll dimer and ionized amino acid side chains.

complexes. A 100-fold difference in rate can be readily explained by differences on the order of 3.3 Å in the electron-tunneling distance between P and the heme edges (Moser et al., 1992). The data in Table I provide criteria for developing a molecular model for the assembly of reaction center–cytochrome complexes. The ability to eliminate all of the first-order kinetic components with high ionic strength (e.g., > 0.2 M NaCl) argues for the importance of electrostatics in the formation of these complexes. We have used the program Delphi, which uses a finite-difference method to find solutions to the linearized Poisson–Boltzmann equation (Gilson & Honig, 1988; Gilson et al., 1985; Gunner & Honig, 1991; Nicholls & Honig, 1991) to characterize the electrostatic properties of the *Rb. sphaeroides* reaction center and *c*-cytochromes.

Rb. sphaeroides Reaction Center. Figure 5A shows the peptide backbone of the *Rb. sphaeroides* reaction center (10^5 MW). The positions of the glutamate, aspartate, lysine, and arginine residues are shown in Figure 5B. The membrane-spanning portion of the reaction center is associated with the region without charged residues (Allen et al., 1987; Deisenhofer & Michel, 1989; Roth et al., 1991; Yeates et al., 1987). The reaction center has an approximate symmetry axis that runs through the middle of the protein, parallel to the membrane-spanning direction. The position of the bacteriochlorophyll dimer is also shown in Figure 5B. The surface of the reaction center that contains the cytochrome binding domain is on top of the views shown in Figure 5. We have previously noted that the cytochrome binding domain is likely to be shifted toward the M-side (left in Figure 5) of the reaction center due to the symmetry-breaking clustering of charged residues on this side (Tiede & Chang, 1988). Figure 5C shows the –3-kT energy surface (assuming a positive test charge) calculated for the reaction center. The region above and to the left of the dimer can be seen to be a region of strong negative potential. However, while this view provides insight into possible trajectories for study of association dynamics, we have found that another format is more useful for identifying likely electrostatic interaction domains in docked complexes.

Figure 6 shows three views of an encounter surface for the reaction center. This surface was calculated by tracing the structure with a 5-Å-radius probe. This surface approximates the closest approach for a collision between the reaction center and a cytochrome that is not sensitive to the precise conformation of the amino acid side chains. Figure 6A shows the encounter surface viewed perpendicular to the symmetry axis. The single H-subunit transmembrane helix is in the center front and is labeled HA. The L- and M-subunits are on the right and left, and the periplasmic and cytoplasmic surfaces are on the top and bottom, respectively. The locations of the L and MA-helices are labeled as LA and MA. This reaction center orientation is the same as shown in Figure 5A and has been well-described (Allen et al., 1986, 1987; Chang et al., 1991; Deisenhofer & Michel, 1989; Tiede et al., 1988). The encounter surface is colored according to the value of the electrostatic potential at each point. The red and blue regions mark areas on this surface where the electrostatic potential is ≤ -3 and ≥ 3 kT, respectively. Intermediate potential values are scaled in yellow and light blue. The direction of the net dipole moment is marked by the dotted red line transecting this volume. The negative pole exits on the reaction center periplasmic surface, and the positive pole exits on the cytoplasmic surface. The projection of the dipole along the P to Q_A direction is greater than along the P to Q_B direction.

Figure 6B shows the portion of the reaction center encounter surface exposed to the cell periplasm, viewed along the symmetry axis. This contains the *c*-cytochrome binding domain. The location and orientation of P underneath this surface are indicated by the bacteriochlorophyll macrocycles drawn in white. This view also shows the exit of the negative pole of the dipole, marked by the dotted line.

Figure 6 provides a complete description of the electrostatic interaction between the reaction center and an idealized molecule of 5-Å radius with uniform charge. The regions in red mark locations of low potential energy for a positively charged ion and function as electrostatic binding sites. The

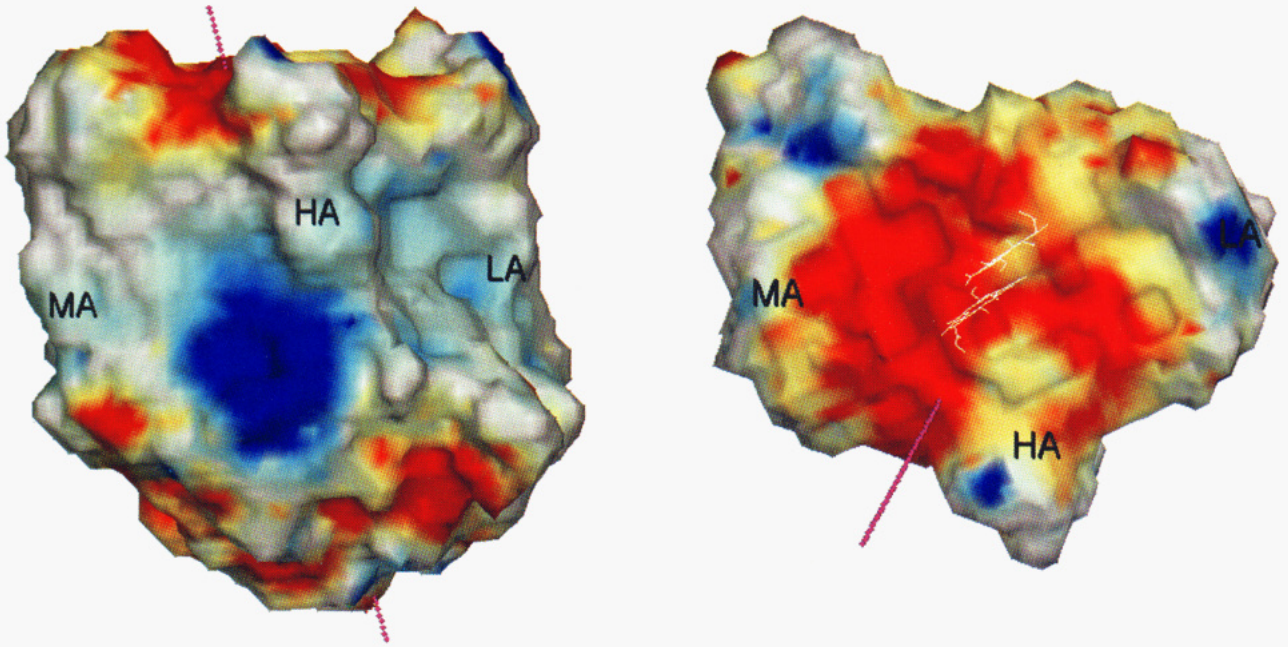

FIGURE 6: Electrostatic potentials mapped onto an encounter surface of the *Rb. sphaeroides* reaction center. Two views of the reaction center encounter surface are shown. Part A (left) shows the encounter surface viewed with the reaction center positioned as shown in Figure 5A. The locations of the transmembrane A-helices of the L- and M-subunits are indicated, along with the location of the single H-subunit transmembrane helix. The encounter surface is colored according to the electrostatic potential on the surface. Regions with potentials of >3 and <–3 kT are marked by blue and red, respectively. Potential values between 0 and 3 kT, and 0 and –3 kT, are scaled between white and blue, and white and red, respectively. The dotted line marks the position of the dipole vector; the negative pole exits on the periplasmic surface (top in figure), and the positive pole exits on the cytoplasmic surface (bottom in figure). Part B (right) shows the periplasmic surface of the reaction center encounter surface that contains the cytochrome *c* binding site. The location and orientation of P underneath this surface are indicated by the superimposed bacteriochlorophyll dimer structure drawn in white. This view of the encounter surface also shows the exit of the negative pole of the dipole vector, marked by the dotted line.

periplasmic surface of the reaction center is seen to only have a broad binding site for cationic molecules, while the cytoplasmic surface has a number of possible anion and cation binding sites. Electrostatic interactions with the *c*-cytochromes will be complicated by their anisotropic shape and charge distributions.

c-Cytochromes. Previously, electrostatic isopotential surfaces have been calculated for horse, tuna, *P. aeruginosa*, and *Rs. rubrum* cytochromes (Matthew, 1985; Northrup et al. 1990; Weber & Tollin, 1985) using analogous finite-difference methods to the linearlized Poisson–Boltzmann equation as described here. In this paper we have calculated the electrostatic potential maps for the remaining cytochromes listed in Table I. In addition, we have shown how the electrostatic potentials map onto encounter surfaces for each cytochrome. This presentation identifies likely electrostatic interaction domains on the cytochromes. The electrostatic characteristics of the encounter surfaces for the *c*-cytochromes were carried out using various atom charge sets as described under Materials and Methods. The results shown in Figures 7 and 8 used the CHARMM charge set for the protein atoms (including added hydrogens), and the heme atoms were assigned charges according to Northrup et al. (1981).

Dipole moments were also calculated for each of the cytochromes (Koppenol & Margoliash, 1982; Northrup et al., 1986). The position of the dipole moment with respect to the center of mass is also shown for the cytochromes in Figure 7 and 8. The direction of the cytochrome dipole moments provides a crude indication of the direction along which the electrostatic potential diminishes most slowly with increasing distance from the encounter surface. The magnitude of the dipole vector provides a measure of the anisotropy in the charge distribution for each cytochrome. As described under Materials and Methods, the charge anisotropy can be broken down further, by calculating the positive, $|\mu_+|/\Sigma q_+$, and negative $|\mu_-|/\Sigma q_-$, charge moments. The normalization yields a parameter for charge clustering that is independent of the total number of charged atoms. The *c*-cytochrome dipole and charge moments are listed in Table II.

For all cytochromes, the encounter surfaces are shown viewed directly at the exposed heme edge, along the Fe atom to heme pyrrole C4C atom direction. The position where the Fe–C4C direction intersects the encounter surface is marked with a cross. The C-pyrrole ring is the most solvent exposed portion of the heme. The Fe–C4C direction lies in the heme plane and passes closest to the thioether link analogous to Cys-17 in the horse sequence. Molecular orbital calculations have found that heme π orbitals are delocalized significantly onto the bridging cysteinyl sulfur atoms and that this represents the closest approach of the heme π system to the solvent (Tollin et al., 1986). For comparison to a cytochrome structure, this same view is shown in Figure 7A for the *Rb. capsulatus* cytochrome c_2. The heme edge is positioned vertically, with the histidine and methionine ligands on the right and left, respectively. In the following discussion, references to positions on the encounter surface are made with respect to the heme position in this orientation for the cytochrome.

The electrostatic map calculated from the *Rb. capsulatus* cytochrome c_2 crystal structure is shown in Figure 7B,C. Figure 7B shows the encounter surface for the front surface of the cytochrome. The most dominant feature of this surface is the area of strong positive potential (>3 kT) located, in this view, below and to the left of the heme crevice. Residues underneath this patch include lysines-54, -84, -93, and -99. The positions of the NZ atoms for these residues are indicated in the figures. This region complements the region of negative potential associated with the cytochrome binding domain on the reaction center surface. In contrast, the back side of the cytochrome, Figure 7C, shows areas of predominately negative potential. The direction of the dipole vector shows that, at distances

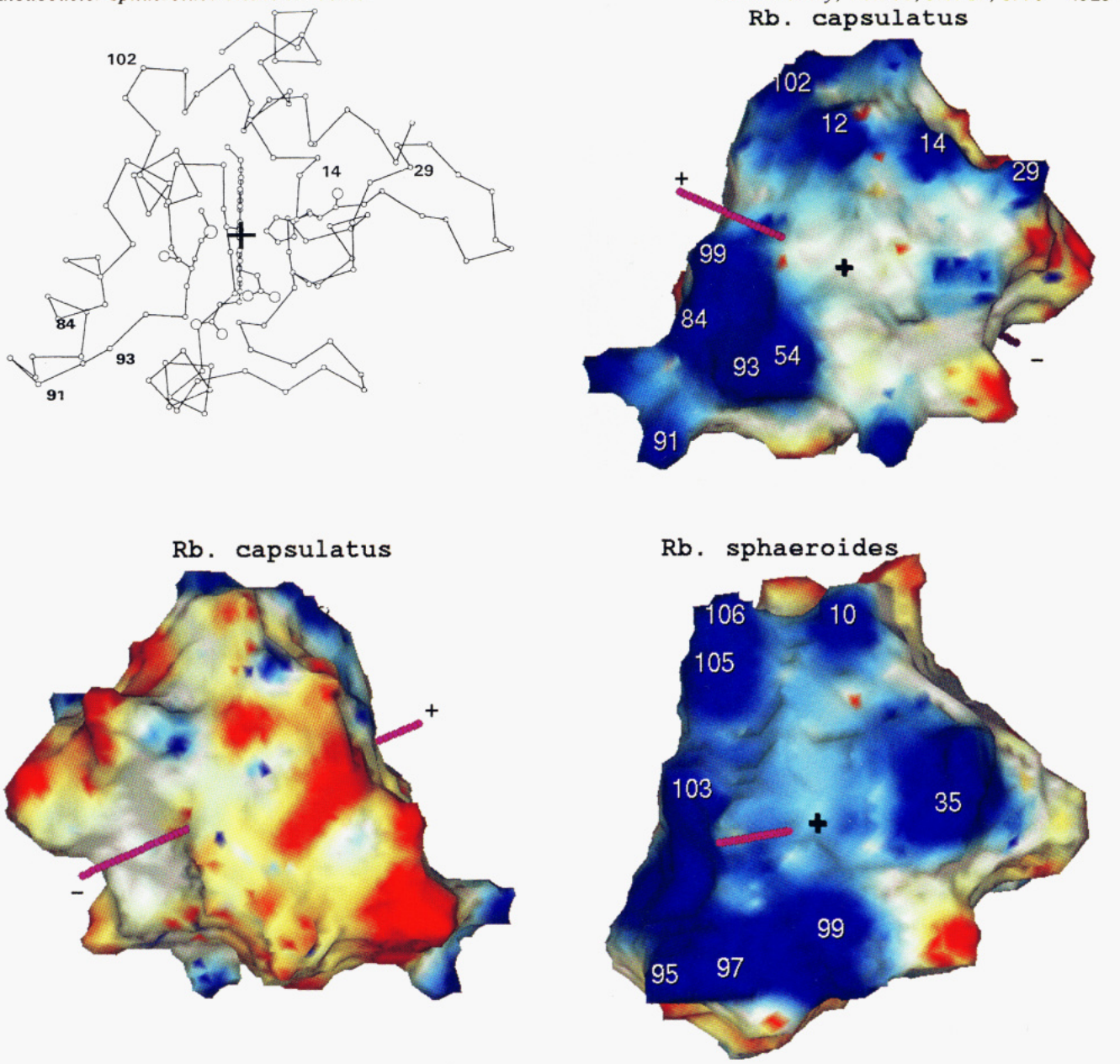

FIGURE 7: Electrostatic potential maps of the *Rb. capsulatus* and *Rb. sphaeroides* cytochromes c_2. Part A (top left) shows the atomic structure of the *Rb. capsulatus* cytochrome, viewed along the heme Fe atom to C4C atom direction. The end-on view of the Fe–C4C atom direction is marked by a cross as it is in the subsequent views of the cytochrome encounter surfaces. The heme is vertical, and viewed edge on, with the histidine and methionine ligands on the right and left, respectively. The positions of the α-carbon atoms for lysine-14, -29, -84, -91, -93, and -102 are marked. This orientation is the same for all the subsequent views of the cytochrome encounter surfaces (expect for part C). Part B (top right) shows the *Rb. capsulatus* cytochrome c_2 encounter surface, viewed with the cytochrome in the same orientation as shown in part A. The Fe to C4C atom direction is marked with the cross. Red and blue mark areas where the electrostatic potential is <-3 and >3 kT, respectively. Potential values between 0 and 3 kT, and 0 and -3 kT, are scaled between white and blue, and white and red, respectively. The direction of the dipole moment is indicated by the line intersecting the encounter surface. The numbers mark the location of the NZ atoms of specific lysine residues underneath the encounter surface. Part C (bottom left) shows the encounter surface for the *Rb. capsulatus* cytochrome, viewed along the heme Fe to C4C direction but from the back of the molecule. The cytochrome is rotated 180° from the view in part B. Part D (bottom right) shows the electrostatic potentials calculated for the *Rb. sphaeroides* cytochrome, mapped onto its encounter surface. The color scheme and other markings are as described above.

away from the encounter surface, the region to the left of the heme edge will continue to have the strongest positive potential, and the regions of negative potential are located on the back of the molecule.

The electrostatic map calculated for the model of the *Rb. sphaeroides* cytochrome c_2 (Figure 7D) shows similar features. The region of strongest positive potential on the encounter surface is located below and to the left of the heme. Residues underneath this patch include Lys-95, -97, -99, and -103. The direction of the dipole moment also shows that the regions just to the left of the heme edge will continue to have the greatest positive potential at distances away from the encounter surface. The negative potential regions are located on the back side of the cytochrome. The similarity of the electrostatic properties of these cytochromes parallels the similar electron-transfer capacities with the reaction center.

For the *Rb. capsulatus* and *Rb. sphaeroides* cytochromes, the position of the positive end of the dipole was found not to accurately track the location of the region of strongest positive potential on the encounter surfaces. This is seen in Figure 7B,D by the intersection of the dipole outside of the regions of strongest positive potential. This result can be understood from the fact that the dipole is the vector sum of the location of all charges, while Coulomb's law weights the contribution

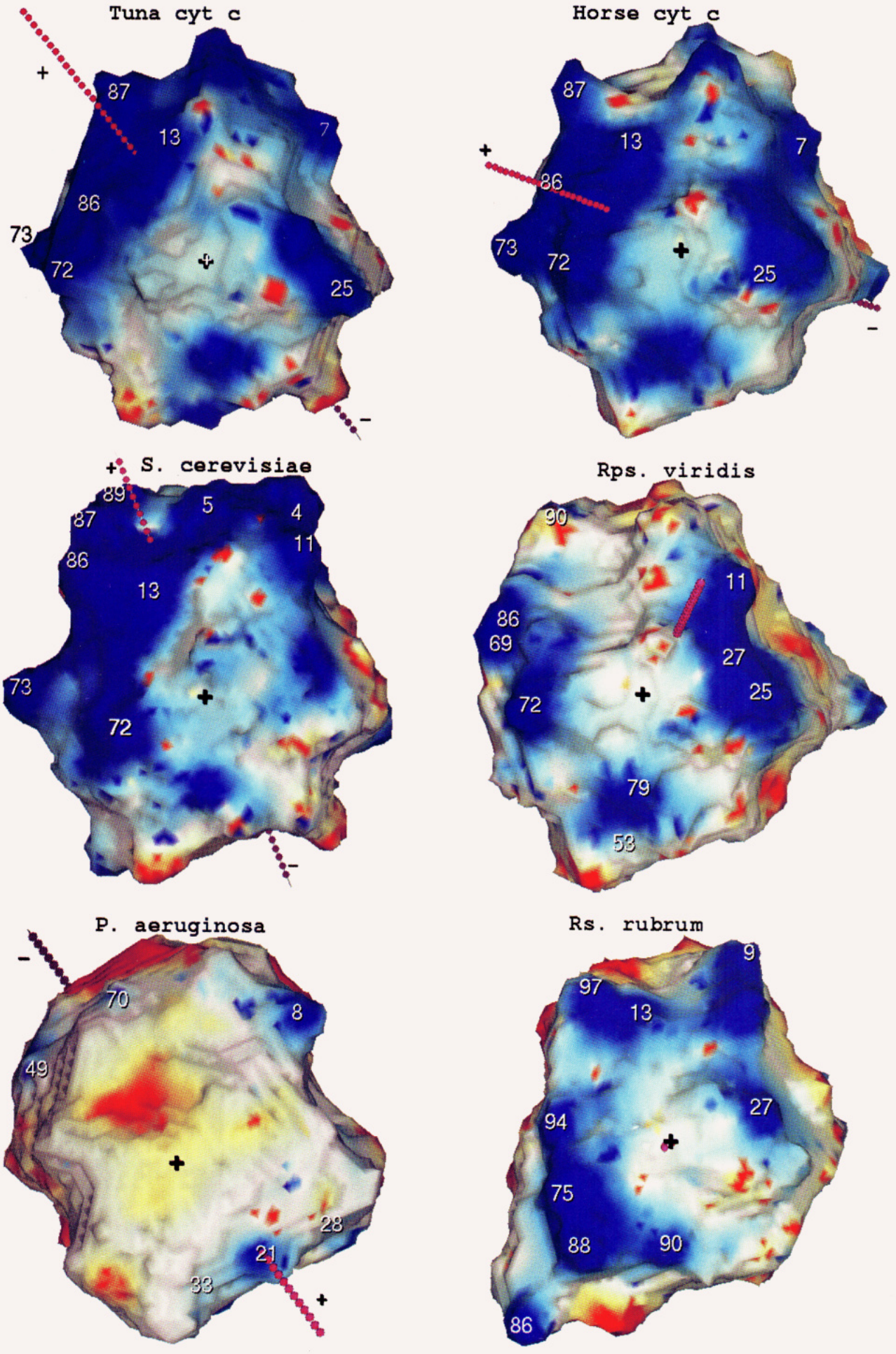
Tuna cyt c
+
87
13
7
86
73
72
25
–
Horse cyt c
87
13
7
+
86
73
72
25
–
+
S. cerevisiae
89
87
5
4
11
86
13
73
72
–
Rps. viridis
90
11
86
69
27
25
72
79
53
P. aeruginosa
–
70
8
49
28
21
33
+
Rs. rubrum
9
97
13
27
94
75
88
90
86

FIGURE 8: Electrostatic potentials mapped onto encounter surfaces for *c*-cytochromes. Parts A–C (top left, top right, middle left) show the electrostatic maps for the mitochondrial cytochromes *c* from tuna, horse, and *S. cerevisiae*, respectively. Parts D–F (middle right, bottom left, bottom right) show the electrostatic maps for the cytochromes that do not form productive 1:1 electron-transfer complexes with the reaction center. Part D shows the electrostatic map for *Rps. viridis* cytochrome c_2; part E, *P. aeruginosa* cytochrome *c*-551; and part F, *Rs. rubrum* cytochrome c_2. In each case, the encounter surface is viewed along the heme Fe to C4C atom direction as described in Figure 7, and other markings are as described in Figures 6 and 7.

Table II: Electrostatic Properties of *c*-Cytochromes

species	net charge[a]	no. of (+) residues[a]	no. of (–) residues[a]	$\lvert\mu_+\rvert/\Sigma q_+$[b] (Å)	$\lvert\mu_-\rvert/\Sigma q_-$[b] (Å)	$\lvert\mu_D\rvert$ (D)	θ_D[c] (deg)
sphaeroides	–2	16	16	0.28	0.67	687	17
capsulatus	0	18	16	0.33	0.51	529	32
tuna	+6	18	9	0.31	0.55	370	66
horse	+6	21	12	0.20	0.49	283	39
cerevisiae	+6	19	11	0.56	0.46	554	72
rubrum	–1	17	16	0.13	0.50	345	1
viridis	+1	15	12	0.25	0.54	274	21
aeruginosa	–3	9	10	0.58	0.86	167	49

[a] No. of (+) residues refers to the number of lysine and arginine residues; no. of (–) residues refers to the number of glutamate and aspartate residues. The heme charge set (Northrup et al., 1981) yields a charge of –2 for the heme group due to the two propionic acids. Differences between the net charge and the sum of the positive, negative, and heme residues are due to species differences in the acetylation of the N-terminus. Each of the charge sets used in the electrostatic potential calculations yielded the same net charge, although the charge and dipole moments changed. The values shown in the table reflect the CHARMM charge set for the protein atoms. [b] $\lvert\mu_+\rvert/\Sigma q_+$ and $\lvert\mu_-\rvert/\Sigma q_-$ are the positive and negative charge moments, normalized for total positive and negative charge. A uniform charge distribution would yield a moment of 0 Å. [c] Angle between the dipole moment and the heme Fe atom to C4C atom direction.

of remote charges to the electrostatic potential by the inverse of the distance. This makes the dipole moment more sensitive to the presence of remote charged atoms. We have seen this property in calculations of electrostatic potential and dipole moments with different atom charge sets. The dipole direction was found to shift by 10°–20°, depending upon whether only terminal acidic and basic residues were assigned charges and whether heme atoms or C- and N-terminal charges were included. Significantly, with each of these charge sets the region of strongest positive potential remained in the same position as shown in the Figure 7. This emphasizes the importance of the clustering of charged residues to produce restricted regions of strong potential. Similar shifts in the direction of the dipole moment were previously calculated for horse cytochrome *c* with different charge sets (Northrup et al., 1986).

A different pattern of electrostatic potential was calculated from the crystal structures of the three cytochromes that exhibited predominately tens of microseconds first-order kinetics. The front view of the encounter surfaces, along the Fe to heme atom C4C directions, for the tuna, horse, and *S. cerevisiae* cytochromes are shown in parts A, B, and C of Figure 8, respectively. In each case the region of strongest positive potential, which complements the negative potential on the reaction center surface, is located above and to the left of the heme crevice. For both tuna and horse cytochromes, this region includes lysines-13, -72, -73, -86, and -87. The shift to the top of the heme crevice is the greatest for *S. cerevisiae* cytochrome *c*. The area of strongest positive potential is broader and includes Lys-4, -5, -11, -13, -72, -73, -86, -87, and -89. The location of the NZ atoms of these residues is marked in Figures 8. The positive portion of the dipole moment is seen to roughly track the location of the patch of strongest positive potential more closely with the mitochondrial cytochromes than it does with the bacterial cytochromes c_2. This is largely a result of large, excess positive charge of the mitochondrial cytochromes (Table II). The clustering of excess positive charge largely determines both the location of strongest positive potential and the direction of the dipole moment. The number of charged residues is similar for the three mitochondrial cytochromes, as seen by the list in Table II. However, a comparison of the positive charge moments shows that the *S. cerevisiae* cytochrome differs from the horse or tuna cytochrome by having a less uniform distribution of positively charged residues. This is reflected in the larger magnitude of the dipole moment, listed in Table II, for the *S. cerevisiae* cytochrome compared to the horse and tuna cytochromes.

The pattern of electrostatic potential calculated from a model of the *Rps. viridis* cytochrome c_2 (Figure 8D) differs markedly from the previous cytochromes that form 1:1 electron-transfer complexes with the reaction center. The major difference is that the charge distribution on the *Rps. viridis* cytochrome does not produce an area of strong positive potential on the left side of the heme. The three small patches of positive potential are seen on the encounter surface. These are situated above single lysine residues. The largest, but still comparatively small, region of positive potential is situated to the right of the heme crevice. The shift in the location of net positive charge is also reflected by the shift in the direction of the dipole moment to the right side of the heme.

Calculations of the electrostatic potential maps from the crystal structure of the cytochrome *c*-551 from *P. aeruginosa* are shown in Figure 8E. This cytochrome exhibits no capacity for electron transfer with the reaction center. The electrostatic map shows that there are no areas of strong positive potential on the front surface of the cytochrome. The electrostatic potential on the encounter surface just above and to the left of the heme cleft is weakly negative. This can account for repulsive collisions with the reaction center cytochrome binding site with cytochrome orientations that are expected to be conducive for electron transfer.

A comparison of the electrostatic maps with the electron-transfer capacities suggests a correlation between the presence of an area of positive potential on the left side of the heme edge and the ability to form a productive electron-transfer complex with the reaction center. However, one exception was found. The electrostatic map calculated from the *Rs. rubrum* crystal structure (Figure 8F) is qualitatively similar to those of the *Rb. sphaeroides* and *Rb. capsulatus* cytochromes. The electrostatic maps for *Rs. rubrum* cytochrome shows a similar region of strong positive potential below and to the left of the heme edge, although the kinetics reported for this cytochrome differ significantly from those of the *Rb. sphaeroides* and *Rb. capsulatus* cytochromes. One possible difference is that regions of positive potential on the left side

of the heme appear to be somewhat smaller on the *Rs. rubrum* encounter surface than for *Rb. capsulatus* and *Rb. sphaeroides*. A comparison of the charge moments shows that this is likely a consequence of a slightly less complete clustering of positively charged residues for the *Rs. rubrum* cytochrome. The diminished charge clustering is also reflected in the smaller dipole moment for the *Rs. rubrum* cytochrome compared to those from *Rb. capsulatus* and *Rb. sphaeroides*. However, as discussed below, the energetic consequences of these differences must await more detailed calculations with the various docked structures.

Table II lists the net charge and dipole moments calculated for the different cytochromes using the atom charge sets described under Materials and Methods. Values for the tuna, horse, and *P. aeruginosa* cytochromes are consistent with those reported previously using similar charge sets (Dixon et al., 1989; Koppenol & Margoliash, 1982; Northrup et al., 1986). Further discussion of the comparison between kinetic and electrostatic properties of the *c*-cytochromes is given below.

DISCUSSION

Kinetic Model

We have found that the first-order time constants are the most reproducible, characteristic features of the electron transfer between the reaction center and a series of water-soluble *c*-cytochromes. This consistency suggests that these kinetic components are intrinsic features of the reaction center–cytochrome interaction. The resolution of multiple first-order components in the fast kinetic phase for several cytochromes suggests that these cytochromes can form multiple productive electron-transfer complexes with the reaction center.

In contrast to the reproducibility of the first-order kinetics, considerable variation was seen in the presence of slower, higher order kinetic components that reach a pseudo-first-order rate limit at high cytochrome concentration. For all cytochromes except for horse and *C. krusei* cytochromes *c*, titrations were observed that identified a two-state equilibrium between free and bound states as the simplest kinetic model. Even for the horse and *C. krusei* cytochromes, the variability in the extent of the pseudo-first-order cytochrome oxidation suggests that this mode of binding to the reaction center is not necessarily an intrinsic feature of the reaction center–cytochrome interaction. The presence of this kinetic component appears to be subject to experimental variation. Although we have not identified the source of this variation, it appears to be linked to the physical state of the reaction center.

A supercomplex organization for the reaction center has been proposed to account for the complex kinetic pattern observed in vivo (Joliot et al., 1989, 1990; Lavergne & Joliot, 1991). In this model, the reaction centers are proposed to be dimerized in such a manner that the binding of cytochrome to one reaction center prevents binding at the other (Joliot et al., 1989, 1990; Lavergne & Joliot, 1991). This proposal provides a conceptual model showing how reaction center dimerization can force cytochrome oxidation to follow a three-state kinetic scheme with only one type of cytochrome binding site. Although it is not clear whether this interpretation can be applied to the in vitro kinetics, this model is one example of how the aggregation state of the reaction center can affect cytochrome oxidation kinetics, without altering the physical basis for the reaction center–cytochrome interaction. Preliminary analysis of small angle neutron scattering experiments shows that reaction centers in LDAO detergent solutions are at least partially aggregated and are likely to exist in a distribution of aggregation states (Thiyagarajan & Tiede, 1990). Although other properties of the reaction center may also be changing, these experiments raise the possibility that variations in the aggregation state of the reaction center in vitro may be linked to the variations in the slow cytochrome oxidation kinetics.

It is important to emphasize that, in spite of the variation found in the minor, slow kinetic components, the major portion of the cytochrome oxidation at saturation occurs by a rapid, first-order reaction in vitro. The rapid, first-order kinetic time constants are invariant in different experiments, and these time constants are found to be intrinsic, characteristic features of specific reaction center–cytochrome pairs.

Origin for Differences in Characteristic Electron-Transfer Times. Characteristic first-order electron-transfer times for the listed cytochromes differed by nearly 2 orders of magnitude, ranging from 0.5 to 40 μs. Second-order rate constants ranged from 10^9 to $<10^1$ M^{-1} s^{-1}. The absence of a correlation between electron-transfer characteristics and the redox potential of the different cytochromes shows that the variation in driving force for the reaction is not likely to be responsible for the variation in rate. Instead, the characteristic first-order electron-transfer times are likely to reflect different structural constraints imposed by the individual reaction center–cytochrome complexes. The kinetic data in this paper can be used as a guide to develop molecular models for reaction center–cytochrome *c* association that account for the differences in cytochrome docking to the reaction center.

Electrostatic Docking Model

The ability to eliminate the first-order kinetic components for all cytochromes at high ionic strength indicates that the reaction center–cytochrome electron-transfer complexes are likely to be primarily stabilized by electrostatic interactions. The electrostatic calculations described in this paper are the first step in developing a quantitative model of the molecular interactions between the reaction center and the *c*-cytochromes. The mapping of electrostatic potentials onto encounter surfaces of the reaction center and *c*-cytochromes identifies likely interaction domains. For the reaction center, the *c*-cytochrome binding domain is found to be nearly exclusively of net negative potential (<3 kT) that is shifted slightly toward the M-subunit side of the reaction center. The cytochromes that are capable of electron transfer to the reaction center show complementary regions of strong positive potential near the heme edge. One striking correlation is seen in the location of these electrostatic interaction domains on the *Rb. sphaeroides* and horse cytochromes and the interaction domains predicted previously from optical dichroism measurements (Tiede, 1987).

Previous dichroism measurements showed that the horse and *Rb. sphaeroides* cytochromes differed in their orientation in electron-transfer complexes formed with the reaction center (Tiede, 1987). The dichroism measured for the *Rb. sphaeroides* cytochrome c_2 predicted that the surface facing the reaction center was essentially that shown in Figure 7. The orientation for the horse cytochrome was measured to be different. Compared to the *Rb. sphaeroides* cytochrome, the interaction domain for the horse cytochrome was rotated by 8° further away from the heme plane and rotated by 32° toward the top of the heme crevice. This location matches closely the region of maximum positive potential shown in Figure 8B.

Preliminary docking studies show that minimum energy configurations for the reaction center–cytochrome complexes will occur when the areas of strong positive potential are positioned over the area of strong negative potential on the

reaction center. In doing this with the *Rb. sphaeroides* and *Rb. capsulatus* cytochromes, the shapes of the proteins and the locations of the area of positive potential cause the surface similar to the views shown in Figure 7B,D to be facing the reaction center. This configuration places the heme edge, with the thiol bridge to Cys-19 (homologous to Cys-17 in the horse sequence), directly over the reaction center. In contrast, placement of the region of strongest positive potential for the horse cytochrome on top of the reaction center interaction domain causes the surface above and to the left (with respect to the cytochrome orientations in Figures 7 and 8) of the heme edge to be facing the reaction center. This configuration rotates the heme edge away from the reaction center, which is in agreement with the dichroism measurements and the slower electron-transfer kinetics for the complex formed with the horse cytochrome compared to the *Rb. sphaeroides* cytochrome.

This correspondence between the locations of regions of positive potential and the dichroism and kinetic measurements for the horse and *Rb. sphaeroides* cytochromes leads us to propose a mechanism for the formation of reaction center–cytochrome electron-transfer complexes that is primarily driven by the justaposition of regions of delocalized complementary potential. In this mechanism the clustering of charged residues is of primary importance and not the location of specific residues. A consequence of this mechanism is that many different sets of charge distributions are capable of stabilizing a specific configuration for a reaction center–cytochrome complex. This mechanism lessens the importance of the location of specific charged residues in the protein sequences and provides an explanation for the lack of a correlation between electron-transfer rates and coincident lysine positions in aligned protein sequences (Long et al., 1989; Tiede & Vashishta, 1991).

Once in a docked structure, the clustering of charged residues allows many configurations to have different pairs of residues associated in complementary charge pairs. We have seen this effect in preliminary docking studies. Once a cytochrome is positioned on the reaction center, there are many different small rotations that yield configurations of approximately equivalent stabilization (C. H. Chang and D. Tiede, unpublished results). Similar observations have been previously made for the cytochrome *c*–cytochrome b_5 complex (Burch et al., 1990; Mauk et al., 1986). Side-chain reorganization in docked complexes (Wendoloski et al., 1987) will significantly increase the possibilities for the formation of different sets of charge pairs, particularly given the size and flexibility of the lysine, arginine, glutamate, and aspartate side chains.

Apart from the *Rs. rubrum* cytochrome, an assembly mechanism primarily driven by delocalized electrostatic domains appears to account for the ordering of the cytochromes in terms of electron-transfer efficacy to the reaction center. All of the cytochromes that form productive 1:1 electron-transfer complexes with the reaction center have the region of strongest positive potential on the left side of the heme cleft. Overlapping the regions of strongest positive potential for the tuna, horse, and *S. cerevisiae* cytochromes on top of the reaction center would cause the heme edge to rotate away from the reaction center. This can be expected to slow the rate of electron transfer with respect to the *Rb. capsulatus* and *Rb. sphaeroides* cytochromes. The shift away from the heme edge is the most severe for the *S. cerevisiae* cytochrome *c*, which is in accord with the slowness of its electron transfer compared to the other cytochromes.

The *Rps. viridis* cytochrome differs from the others in that the regions of strong positive potential are to the right and below the heme cleft. Presumably, binding in this orientation does not permit rapid first-order electron transfer. Finally, the absence of electron transfer with the *P. aeruginosa* cytochrome can be understood from the absence of regions of strong positive potential surrounding the heme edge. Optical dichroism measurements for the different reaction center–cytochrome complexes will provide a means of verifying the orientations predicted by the regions of strong positive potential on the encounter surfaces.

The similarity of the electrostatic potential maps for the *Rs. rubrum*, *Rb. sphaeroides*, and *Rb. capsulatus* cytochromes suggests that the electron-transfer kinetics ought to be similar for all three. The reported pronounced difference in electron-transfer characteristics for the *Rs. rubrum* cytochrome (Long et al., 1989) contradicts the qualitative similarity found here between the *Rs. rubrum* and the *Rb. capsulatus* and *Rb. sphaeroides* cytochromes. One possible explanation for the contradiction is that a rapid ($\tau < 1$ μs) electron transfer of the *Rs. rubrum* cytochrome in a 1:1 complex with the reaction center was missed in the earlier work. However, this appears unlikely because the time resolution reported in these experiments was sufficient to detect such a rapid electron transfer (Long et al., 1989). A reevaluation of the electron-transfer kinetics with *Rs. rubrum* cytochrome c_2 is currently underway. Another possibility is that the ability to form a productive 1:1 complex with the reaction center may be sensitive to more subtle electrostatic characteristics of the cytochromes. One difference was noted between the electrostatic maps of the *Rs. rubrum* and the *Rb. capsulatus* and *Rb. sphaeroides* cytochromes. The *Rs. rubrum* cytochrome appears to have a slightly smaller extent of net positive charge clustering on the left side of the heme edge. This is reflected in the slightly smaller area of the region of greatest positive potential and smaller dipole moment with respect to the *Rb. capsulatus* and *Rb. sphaeroides* cytochromes. Possibly, the positive potential on the front surface of the *Rs. rubrum* cytochrome falls below a threshold needed to stabilize a productive electron-transfer complex. A quantitative model of reaction center–cytochrome association is currently being developed to evaluate differences in the energy of stabilization for the different docked complexes.

It is noteworthy that cytochromes c_2 from *Rs. rubrum* (Hall et al., 1987a; Rickle & Cusanovich, 1979; Van der Wal et al., 1987) and *Rps. viridis* (Knaff et al., 1991) do not show rapid, first-order reactions when oxidized by their physiological oxidants, the *Rs. rubrum* reaction center, and the cytochrome subunit of the *Rps. viridis* reaction center, respectively. Neither the cytochrome c_2 nor the reaction center from *Rs. rubrum* appears to be optimized for electron transfer. This conclusion is suggested by observations that horse cytochrome *c* is a faster reductant for the *Rs. rubrum* reaction center than is the physiological partner *Rs. rubrum* cytochrome c_2 (Van der Wal et al., 1987) and that the *Rs. rubrum* reaction center is a less efficient oxidant of both *Rs. rubrum* cytochrome c_2 and horse cytochrome *c* than is the *Rb. sphaeroides* reaction center [compare data in Hall et al. (1987a,b), Long et al. (1989), and Van der Wal et al. (1987)]. Apart from the discussion in the preceding paragraph, there is no explanation for these differences.

Comparison to Previous Models for Reaction Center–Cytochrome Association. Two models of the *Rb. sphaeroides* reaction center–cytochrome complex have been built on the basis of the X-ray structure of the *Rb. sphaeroides* reaction

center (Allen et al., 1987; Tiede et al., 1988; Tiede & Chang, 1988). While the two models differ in many respects (Tiede et al., 1988; Tiede & Chang, 1988), both models are based upon the assumption that the reaction center–cytochrome complex is primarily held together by a collection of complementary charge pairs or salt bridges between specific residues on the reaction center and cytochrome surfaces. These models imply a specific role for each of the interacting amino acid residues. However, there is little experimental support for such a specific role.

Chemical modification of single lysine residues has been used to probe the interaction domains on *Rb. sphaeroides* cytochrome c_2 and horse cytochrome *c* surfaces for binding to the *Rb. sphaeroides* reaction center (Hall et al., 1987b; Long et al., 1989; Van der Wal et al., 1987). Dramatic changes in electron-transfer kinetics are induced upon modification of specific residues. However, these changes may be induced by a combination of steric and more delocalized electrostatic perturbations rather than by removal of specific amino acid interactions. There is good agreement between the interaction domains predicted by the optical dichroism, chemical modification, and electrostatic maps reported here [see Tiede and Dutton (1992) for review].

Estimates of the strength of the electrostatic stabilization of the *Rb. sphaeroides* reaction center–*Rb. capsulatus* cytochrome c_2 complex have been made by modeling the ionic strength dependence of the second-order rate constant (Caffrey et al., 1992). The electrostatic interaction energy was determined for the wild-type cytochrome c_2 and three single-site mutants where lysine residues (12, 14, and 32) were converted to glutamate or aspartate residues. The electrostatic interaction energies were interpreted in terms of charge pairing between these residues and specific residues on the reaction center surface (Caffrey et al., 1992). However, an alternate explanation is to interpret the interaction energy as due to the delocalized potential. It is noteworthy that the mutagenesis studies find that the residues on the right side of the heme cleft play a less important role in the electrostatic stabilization than the lysine residue above the heme cleft (Caffrey et al., 1992). This is in keeping with the proposal that the interaction domains for the *Rb. capsulatus* and *Rb. sphaeroides* cytochromes are shifted toward the left side of the heme cleft. The results of both the chemical modification studies and the estimates of electrostatic stabilizations are compatible with the interpretation that the reaction center–cytochrome complexes are primarily stabilized by delocalized electrostatic potentials.

Comparisons to Nonphotosynthetic Systems. Factors controlling bimolecular association and electron transfer have been extensively examined for reactions between soluble *c*-cytochromes and a variety of nonphotosynthetic proteins [for recent reviews, see Kostic (1990), McLendon (1991), and McLendon and Hake (1992)]. This work has led to the general view that the molecular recognition for *c*-cytochromes does not involve a classical lock-and-key mechanism but involves broad patches of complementary charge and hydrophobicity (McLendon, 1991; McLendon & Hake, 1992). The reaction center–cytochrome *c* interaction fits this view. Experiments (Burch et al., 1990) and molecular modeling calculations (Mauk et al., 1986; Northrup et al., 1988; Weber & Tollin, 1985; Wendoloski et al., 1987) indicate that, within a binding domain, there are likely to be many nearly isoenergetic configurations which may be dynamically interconverting. Furthermore, kinetic and electrostatic modeling suggest that there may be multiple electrostatically stabilized complexes, distinguishable by differences in electron-transfer rate (Hoffman et al., 1991; Northrup et al., 1988). The multiple first-order kinetics observed for the reaction center–cytochrome *c* complexes and the preliminary modeling also support this view.

The electron transfer for 1:1 complexes of cytochrome *c* and cytochrome *c* peroxidase (Hahm et al., 1992; Hoffman et al., 1991) and cytochrome *c* and cytochrome b_5 (Willie et al., 1992) shows "gated" kinetics, analogous to the three-state kinetic models described for the reaction center. For the cytochrome *c* peroxidase system, the slow, gated electron transfer appears to be an intrinsic feature of the cytochrome *c*–cytochrome *c* peroxidase interaction (Hahm et al., 1992; Hoffman et al., 1991). This differs from the variability seen in the presence of this mode of interaction with the reaction center. However, like the reaction center, the kinetics of the rapid electron-transfer component with cytochrome *c* peroxidase are dependent upon the species origin of the cytochrome *c* (Hazzard et al., 1987; Ho et al., 1985; Hoffman et al., 1991). Recent NMR measurements also support these results and show that the molecular contacts between cytochrome *c* peroxidase and cytochrome *c* are species dependent (Moench et al., 1992). These findings are in accord with the observations discussed above that the *c*-cytochromes can be distinguished by their characteristic electron-transfer kinetics with the reaction center and by their optical dichroism in 1:1 complexes with the reaction center. Finally, binding constants for the cytochrome *c*–cytochrome b_5 (Mauk et al., 1986; Rodgers et al., 1988), cytochrome *c*–cytochrome *c* peroxidase (Hake et al., 1992), and cytochrome *c*–flavodoxin (Weber & Tollin, 1985) complexes are comparable to those of the reaction center–cytochrome *c* complexes (Moser & Dutton, 1988; Overfield et al., 1979; Rosen et al., 1979) and fall in the range 10^7–10^5 M^{-1} depending upon ionic strength, pH, and preparation. This is consistent with the shared mechanism for molecular interaction in each of these systems.

ACKNOWLEDGMENT

The authors gratefully acknowledge John Kolenko and Ron VanBuskirk (Chemistry Division, ANL) for their excellent, expert support of the molecular graphics hardware and software.

REFERENCES

Abola, E. E., Bernstein, F. C., Bryant, S. H., Koetzle, T. F., & Weng, J. (1987) in *Crystallographic databases—Information content, software systems, scientific applications* (Allen, F. H., Bergerhoff, G., & Sievers, R., Eds.) pp 107–132, Data Commission of the International Union of Crystallography, Bonn, Germany.

Allen, J. F. (1988) *J. Mol. Biol. 204*, 495–496.

Allen, J. P., Feher, G., Yeates, T. O., Rees, D. C., Deisenhofer, J., Michel, H., & Huber, R. (1986) *Proc. Natl. Acad. Sci. U.S.A. 83*, 8589–8593.

Allen, J. P., Feher, G., Yeates, T. O., Komiya, H., & Rees, D. C. (1987) *Proc. Natl. Acad. Sci. U.S.A. 84*, 6162–6166.

Ambler, R. P., Meyer, T. E., Kamen, M. D., Schichman, S. A., & Sawyer, L. (1981) *J. Mol. Biol. 147*, 351.

Bartsch, R. G. (1978) in *The Photosynthetic Bacteria* (Clayton, R. K., & Sistrom, W. R., Eds.) pp 249–279, Plenum Press, New York.

Bernstein, F. C., Koetzle, T. F., Williams, G. J. B., Meyer, E. F., Brice, M. D., Rodgers, J. R., Kennard, O., Shimanouchi, T., & Tasumi, M. (1977) *J. Mol. Biol. 112*, 535–542.

Bhatia, G. E. (1981) Refinement of the crystal structure of oxidized *Rhodospirillum rubrum* cytochrome *c*2, Ph.D. Thesis, University of California, San Diego.

Burch, A. M., Rigby, S. E. J., Funk, W. D., MacGillivray, R. T. A., Mauk, M. R., Mauk, A. G., & Moore, G. R., & Moore, G. R. (1990) *Science 247*, 831–833.
Bushnell, G. W., Louie, G. V., & Brayer, G. D. (1990) *J. Mol. Biol. 214*, 585–595.
Caffrey, M. S., Bartsch, R. G., & Cusanovich, M. A. (1992) *Biochemistry 267*, 6317–6321.
Chang, C.-H., El-Kabbani, O., Tiede, D. M., Norris, J., & Schiffer, M. (1991) *Biochemistry 30*, 5352–5360.
Deisenhofer, J., & Michel, H. (1989) *Angew. Chem., Int. Ed. Engl. 28*, 829–968.
Dixon, D. W., Hong, X., & Woehler, S. E. (1989) *Biophys. J. 56*, 339–351.
Dutton, P. L., & Prince, R. C. (1978) in *The Photosynthetic Bacteria* (Clayton, R. K., & Sistrom, W. R., Eds.) pp 525–570, Plenum Press, New York.
Dutton, P. L., Petty, K. M., Bonner, H. S., & Morse, S. D. (1975) *Biochim. Biophys. Acta 387*, 536–556.
El-Kabbani, O., Chang, C.-H., Tiede, D. M., Norris, J., & Schiffer, M. (1991) *Biochemistry 30*, 5361–5369.
Gilson, M. K., & Honig, B. A. (1988) *Proteins 3*, 32–52.
Gilson, M. K., Rashin, A., Fine, R., & Honig, B. (1985) *J. Mol. Biol. 183*, 503–516.
Gunner, M. R. (1991) *Curr. Top. Bioenerg. 16*, 319–367.
Gunner, M. R., & Honig, B. (1991) *Proc. Natl. Acad. Sci. U.S.A. 88*, 9151–9155.
Hahm, S., Durham, B., & Millett, F. (1992) *Biochemistry 31*, 3472–3477.
Hake, R., McLendon, G., Corin, A., & Holzschu, D. (1992) *J. Am. Chem. Soc. 114*, 5442–5443.
Hall, J., Ayres, M., Zha, X., O'Brien, P., Durham, B., Knaff, D., & Millett, F. (1987a) *J. Biol. Chem. 262*, 11046–11051.
Hall, J., Zha, X., Durham, B., O'Brien, P., Vieira, B., Davis, D., Okamura, M., & Millett, F. (1987b) *Biochemistry 26*, 4494–4500.
Harvey, S. (1989) *Proteins 5*, 79–92.
Hazzard, J. T., Poulos, T. L., & Tollin, G. (1987) *Biochemistry 26*, 2836–2848.
Ho, P. S., Sutoris, C., Liang, N., Margoliash, E., & Hoffman, B. M. (1985) *J. Am. Chem. Soc. 107*, 1070–1071.
Hoffman, B. M., Natan, M. J., Nocek, J. M., & Wallin, S. A. (1991) *Struct. Bonding 75*, 85–108.
Holden, H., Meyer, T., Cusanovich, M., Daldal, F., & Rayment, I. (1987) *J. Mol. Biol. 195*, 229–231.
Joliot, P., Vermeglio, A., & Joliot, A. (1989) *Biochim. Biophys. Acta 975*, 336–345.
Joliot, P., Vermeglio, A., & Joliot, A. (1990) *Biochemistry 29*, 4355–4361.
Knaff, D. B., Willie, A., Long, J. E., Kriauciunas, A., Durham, B., & Millett, F. (1991) *Biochemistry 30*, 1303–1310.
Koppenol, W. H., & Margoliash, E. (1982) *J. Biol. Chem. 257*, 4426–4437.
Kostic, N. (1990) in *Metals in Biological Systems* (Sigel, H., Ed.) pp 129–182, Verlag, New York.
Lavergne, J., & Joliot, P. (1991) *Trends Biochem. Sci. 16*, 129–134.
Long, J. E., Durham, B., Okamura, M., & Millett, F. (1989) *Biochemistry 28*, 6970–6974.
Louie, G. V., & Brayer, G. D. (1990) *J. Mol. Biol. 214*, 527–555.
Louie, G. V., Hutcheon, W. L. B., & Brayer, G. D. (1988) *J. Mol. Biol. 199*, 295–314.
Matsuura, Y., Takano, T., & Dickerson, R. E. (1982) *J. Mol. Biol. 156*, 389.
Matthew, J. B. (1985) *Annu. Rev. Biophys. Biophys. Chem. 14*, 387–417.
Mauk, M. R., Mauk, A. G., Weber, P. C., & Matthew, J. B. (1986) *Biochemistry 25*, 7085–7091.
McLendon, G. (1991) *Struct. Bonding 75*, 159–174.
McLendon, G., & Hake, R. (1992) *Chem. Rev. 92*, 481–490.
Meyer, T. E., & Kamen, M. D. (1982) *Adv. Protein Chem. 35*, 105–212.
Miki, K., Saeda, M., Masaki, K., Kasai, N., Miki, M., & Hayashi, K. (1986) *J. Mol. Biol. 191*, 579–580.
Moench, S. J., Chroni, S., Lou, B.-S., Erman, J. E., & Satterlee, J. D. (1992) *Biochemistry 31*, 3661–3670.
Moser, C. C., & Dutton, P. L. (1988) *Biochemistry 27*, 2450–2461.
Moser, C. C., Keske, J. M., Warncke, K., Farid, R. S., & Dutton, P. L. (1992) *Nature* (in press).
Nicholls, A., & Honig, B. (1991) *J. Comput. Chem. 12*, 435–445.
Northrup, S. H., Pear, M. R., Morgan, J. D., & McCammon, J. A. (1981) *J. Mol. Biol. 153*, 1087–1109.
Northrup, S. H., Reynolds, J. C. L., Miller, C. M., Forrest, K. J., & Boles, J. O. (1986) *J. Am. Chem. Soc. 108*, 8162–8170.
Northrup, S. H., Boles, J. O., & Reynolds, J. C. L. (1988) *Science 241*, 67–70.
Northrup, S. H., Wensel, T. G., Meares, C. F., Wendoloski, J. J., & Matthew, J. B. (1990) *Proc. Natl. Acad. Sci. U.S.A. 87*, 9503–9597.
Overfield, R. E., & Wraight, C. A. (1986) *Photosynth. Res. 9*, 167–179.
Overfield, R. E., Wraight, C. A., & DeVault, D. (1979) *FEBS Lett. 50*, 137–142.
Rickle, G. K., & Cusanovich, M. A. (1979) *Arch. Biochem. Biophys. 197*, 589–598.
Rodgers, K. K., Pochapsky, T. C., & Sligar, S. G. (1988) *Science 240*, 1657–1659.
Rosen, D., Okamura, M. Y., & Feher, G. (1979) *Biophys. J. 25*, 204a.
Rosen, D., Okamura, M. Y., Abresch, E. C., Valkirs, G. E., & Feher, G. (1983) *Biochemistry 22*, 335–341.
Roth, M., Arnoux, B., Ducruix, A., & Reiss-Husson, F. (1991) *Biochemistry 30*, 9403–9413.
Salemme, F. R., Freer, S. T., Xuong, N. H., Alden, R. A., & Kraut, J. (1973) *J. Biol. Chem. 248*, 3910.
Takano, T., & Dickerson, R. E. (1981) *J. Mol. Biol. 153*, 79.
Thiyagarajan, P., & Tiede, D. M. (1990) in *IPNS Progress Report* (Rotella, F. J., Ed.) p 86, Argonne National Laboratory, Argonne, IL.
Tiede, D. M. (1987) *Biochemistry 26*, 397–410.
Tiede, D. M., & Chang, C.-H. (1988) *Isr. J. Chem. 28*, 183–191.
Tiede, D. M., & Vashishta, A.-C. J. (1991) *Mol. Cryst. Liq. Cryst. 194*, 191–200.
Tiede, D. M., & Dutton, P. L. (1992) in *The Photosynthetic Reaction Center* (Norris, J. R., & Deisenhofer, J., Eds.) Academic Press, New York (in press).
Tiede, D. M., Budil, D. E., Tang, J., El-Kabbani, O., Norris, J. R., Chang, C.-H., & Schiffer, M. (1988) in *The Photosynthetic Bacterial Reaction Center* (Breton, J., & Vermeglio, A., Eds.) Vol. 149, pp 13–20, Plenum Press, New York.
Timkovich, R., & Dickerson, R. E. (1976) *J. Biol. Chem. 251*, 4033.
Tollin, G., Hanson, L. K., Caffrey, M., Meyer, T. E., & Cusanovich, M. A. (1986) *Proc. Natl. Acad. Sci. U.S.A. 83*, 3693–3697.
Van der Wal, H. N., Van Grondelle, R., Millet, F., & Knaff, D. B. (1987) *Biochim. Biophys. Acta 893*, 490–498.
Weber, P. C., & Tollin, G. (1985) *J. Biol. Chem. 260*, 5568–5573.
Wendoloski, J. J., Matthew, J. B., Weber, P. C., & Salemme, F. R. (1987) *Science 238*, 794–796.
Willie, A., Stayton, P. S., Sligar, S. G., Durham, B., & Millett, F. (1992) *Biochemistry 31*, 7237–7242.
Wraight, C. A. (1979) *Biochim. Biophys. Acta 548*, 500–515.
Yeates, T. O., Komiya, H., Rees, D. C., Allen, J. P., & Feher, G. (1987) *Proc. Natl. Acad. Sci. U.S.A. 84*, 6438–6442.